The gut contractile organoid: a novel model for studying the gut motility regulated by coordinating signals between interstitial cells of Cajal and smooth muscles

Rei Yagasaki[1,2], Ryo Nakamura[1,3], Yuuki Shikaya[1,4], Ryosuke Tadokoro[1,5], Ruolin Hao[6,7], Zhe Wang[6,7], Mototsugu Eiraku[6,7], Masafumi Inaba[1] and Yoshiko Takahashi[1,8]

1: Department of Zoology, Graduate School of Science, Kyoto University Sakyo-ku, Kyoto 606-8502, Japan
2: Present Address: WPI Nano Life Science Institute (WPI-NanoLSI), Kanazawa University, Kakuma-machi, Kanazawa 920-1192, Japan
3: Present Address: Ushimado Marine Institute, Okayama University, Setouchi, Okayama 701-4303, Japan
4: Present Address: Sorbonne Université, CNRS, Institut de la Mer de Villefranche, UMR7009 Laboratoire de Biologie du Développement de Villefranche-sur-Mer (LBDV), Villefranche-sur-Mer, France
5: Present Address: Department of Bioscience, Okayama University of Science, Okayama, Japan
6: Institute for Life and Medical Sciences, Kyoto University, Sakyo-ku, Kyoto 606-8507, Japan
7: Department of Polymer Chemistry, Graduate School of Engineering, Kyoto University, Kyoto 615-8510, Japan
8: Author to whom all correspondence should be addressed.
email: yotayota@develop.zool.kyoto-u.ac.jp

Keywords:
gut contraction, interstitial cells of Cajal, smooth muscle cells, organoid, gap junction

Abstract

The gut undergoes peristaltic movements regulated by intricate cellular interactions. However, they have poorly been explored due to a lack of model system. We here developed a novel contractile organoid that is derived from the muscle layer of chicken embryonic hindgut. The organoid contained smooth muscle cells (SMCs) and interstitial cells of Cajal (ICCs; pacemaker) with few enteric neurons, and underwent periodic contractions. The organoid formed by self-organization with morphological arrangements of ICCs (internal) and SMCs (peripheral), allowing identification of these cells in live. GCaMP-Ca^{2+} imaging analyses revealed that Ca^{2+} transients between ICC-ICC, SMC-SMC or SMC-ICC were markedly coordinated. Pharmacological studies further showed that gap junctions play a role in ICC-to-SMC signaling, and also possible feedback from SMC's contraction to ICC's pace-making activities. In addition, two organoids with different rhythm became synchronized when mediated by SMCs, unveiling a novel contribution of SMCs to ICC's pace-making. The gut contractile organoid developed in this study offers a useful model to understand the mechanisms underlying the rhythm coordination between/among ICCs and SMCs during gut peristaltic movements.

Introduction

In the gut, ingested material is conveyed properly along the gut axis by the gut movements called peristalsis, which is recognized as wave-like propagation of a local constriction. The physiology of gut peristalsis has extensively been studied in adults, where the peristalsis plays pivotal roles in effective transportation and digestion/absorption of inter-luminal contents. And many cases of gut-related pathology are associated with peristaltic disfunctions. The gut peristaltic movements are achieved by intricate regulations of intercellular functions among multiple cell types. At the site of origin of peristaltic waves (OPW), a local constriction emerges along the circumferential axis, and this is soon followed by a progressive wave of the contraction along the gut axis. During these processes, the circumferential constriction demands multiple SMCs to achieve simultaneous contraction. However, due to the complex structure of the gut, how such synchronization/coordination in SMCs is regulated remains largely undetermined.

It is known in vertebrates that the embryonic gut undergoes peristaltic movements even without experience of food intake. The embryonic gut therefore serves as a powerful model to study the intrinsic mechanisms underlying the peristalsis contrasting with the adult gut where ingested content influences the gut motility increasing complexity in analyses. We have recently reported using chicken embryos that sites of OPW are randomly distributed along the gut axis at early stages, and they later become confined to specific sites, and this confinement of OPWs enables rhythmic and patterned peristaltic movements (Shikaya et al., 2022). One of the long-standing and important questions is how the synchronized/coordinated contraction is achieved.

In a long history of gut motility studies, it has been known that enteric nervous system (ENS), smooth muscle cells (SMCs) and interstitial cells of Cajal (ICCs) play important roles in peristaltic movements (Barajas-Lopez et al., 1989, Camborova et al., 2003, Huizinga et al., 1995, Kito et al., 2005, Liu et al., 1998, Rumessen and Thuneberg, 1996, Sanders et al., 1991, Takaki, 2003, Takayama et al., 2002, Thomsen et al., 1998, Chevalier et al., 2020). It has widely been accepted that: 1) at early embryonic stages, gut movement/peristalsis does not require ENS activity, 2) ICCs serve as a pacemaker dictating their rhythm to SMCs, 3) the contraction is executed by SMC and not by ICCs, since thick fibers of myosin are found solely in SMCs. A series of elaborate electrophysiological studies showed that slow waves (a type of changes in membrane potential characteristic of gut movements) occur intrinsically in ICCs but not in SMCs, and that these slow waves lead to voltage-dependent Ca^{2+} influx evoking action potential, which is somehow transmitted to SMCs to execute gut contraction in register with ICC's pace-making rhythm (Baker et al., 2021, Torihashi et al., 2002). The knowledge that ICCs

85 act as a pacemaker was supported by compelling evidence obtained by c-Kit-deficient
86 mouse mutants (W/W^v), in which ICC differentiation was severely affected leading to a
87 failure of gut peristalsis (Huizinga et al., 1995, Torihashi et al., 1999). However, it
88 remains largely unexplored how the intrinsic/spontaneous rhythm in a single ICC
89 becomes synchronized among multiple ICCs which constitute intricate networks in the
90 gut. It has also been under debate to what extend the gap junction contributes to cell-cell
91 communications between ICCs, SMCs or ICC-SMC. One reason is that it has been
92 difficult to stably maintain SMCs and ICCs in cell culture condition, and also to
93 distinguish ICCs from SMCs in the living gut (these two types of cells originate from the
94 same progenitors of splanchnopleural mesoderm during development). Thus, a novel
95 model system has been awaited to circumvent these obstacles. Recently, it was reported
96 that differentiation states of mouse hindgut-derived cells were successfully maintained
97 for a relatively long period of time in a serum-free culture medium (Wang et al., 2018).
98 In that study, many types of gut-derived cells including not only ENS, ICC, SMCs but
99 also glial cells and serosa were observed, and this large and complex cell mass was seen
100 to undergo rhythmic contractions *in vitro*.
101 It has widely been appreciated that organoids can serve as a powerful models
102 and tools to circumvent such obstacles of organ complexity. Their relatively simple
103 structures allow analyses at higher resolution than *in vivo*, and also permit analyses of cell
104 behaviors in three-dimensional (3D) environment, which might be different from
105 behaviors *in vitro* behaviors confined to two dimensions. In the current study, we have
106 developed a novel organoid called "gut contractile organoid" by culturing chicken
107 hindgut-derived cells in a serum-free medium. The gut contractile organoid undergoes
108 periodic contractions, and it is essentially composed of ICCs and SMCs, the former
109 residing centrally whereas the latter peripherally, allowing distinction between the two
110 cell types in living organoids. These advantages enabled GCaMP-live imaging of Ca^{2+}
111 dynamics and revealed coordinated oscillations of Ca^{2+} transients between ICC-ICC,
112 SMC-SMC and SMC-ICC. Pharmacological studies further suggested that gap junctions
113 play a role in an ICC-to-SMC signaling, and also a possible feedback from SMC's
114 contractions to ICC's pace-making activities. In addition, by regarding a single organoid
115 as an oscillator unit and by placing oscillators separately in a hydrogel mold, we found
116 that two oscillators with different rhythm become synchronized when mediated by SMCs,
117 supporting the notion of SMC' contribution to ICC's pace-making. The gut contractile
118 organoid developed in this study must be useful to unveil the intrinsic mechanisms
119 underlying the rhythm coordination between/among ICCs and SMCs during peristaltic
120 movements in the embryonic gut.

121 **Materials and Methods**

122 **Chicken embryos**

123 Fertilized chicken eggs were obtained from the Yamagishi poultry farms
124 (Wakayama, Japan) and Takeuchi Farm (Nara, Japan). Embryos were staged according
125 to embryonic days. All animal experiments were conducted with the ethical approval of
126 Kyoto University (#202110).

127

128 **Culture preparation of hindgut-derived cells**

129 A hindgut was dissected from E15 chicken embryos (Fig. S1A), and cut into
130 small pieces. After treating with 25 U dispase (Fujifilm Wako, 383-02281) /phosphate
131 buffer saline (PBS: 0.14 M NaCl, 2.7 mM KCl, 10 mM Na_2HPO_4-$12H_2O$, 1.8 mM
132 KH_2PO_4) at 38.5 °C for 40 min, serosa and intestinal epithelium were removed using
133 forceps. The muscle layer was minced into smaller pieces and treated with 0.2 mg/ml
134 collagenase (Fujifilm Wako, 038-22361) and 0.25 % trypsin/PBS at 37.0 °C for 30 min.
135 The reaction was stopped with 1 % FBS/PBS followed by centrifugation at 800 rpm for
136 3 min. The pellet was resuspended and washed in PBS followed by centrifugation. The
137 pellet was resuspended in culture medium, and 5.0×10^5 cells were plated in a glass bottom
138 dish (Matsunami, D11130H) treated with Matrigel (Corning, 354248) prepared in
139 advance at 38.5 °C for 20 min before use. Poly-lysine and collagen-coated dishes were
140 purchased (Matsunami, D11131H, D11134H). D-MEM /Ham's F-12 (Wako, 048-29785),
141 Ham's F-12 (Wako, 087-08335) and Neurobasal medium (Gibco, 21103-049) with 1× B-
142 27 supplement (Gibco, 17504044) and 0.5 mM L-glutamine were tested. After seeding,
143 time-lapse images were obtained with CM20 (Evident) under 5% CO_2 and 38.5°C with
144 2-hour intervals.

145

146 **Assessment of contraction in the spheroid/cluster**

147 The time-lapse images were obtained by confocal microscopy (Nikon, A1R)
148 under 5 % CO_2 and 38.5 °C. The bright field images were converted to the sequence of
149 Tiff images. Using ImageJ (National Institutes of Health, USA), these sequences were
150 divided into foreground and background automatically (Auto Threshold, mode "default")
151 and graphed by Plot Z-axis profile.

152

153 **Immunocytochemistry**

154 An organoid was fixed in acetic acid/ethanol (1:5) for 10 min at room
155 temperature (RT), and washed in PBS for 10 min at RT. The specimens were
156 permeabilized in 0.1% Tween-20 in PBS for 10 min at RT, followed by washing in PBS

157 for 10 min at RT. After blocking with 1 % blocking reagent for 1 hour at RT, specimens
158 were incubated overnight at 4 °C with dilution of 1:300 anti-c-Kit (Yagasaki et al., 2022),
159 1:300 Tuj-1 (RSD, MAB1195), 1:400 anti-αSMA antibody (Sigma-Aldrich, A5228),
160 and/or 1:200 anti-N-cadherin antibodies (TAKARA, M110) in 1% blocking regent
161 (Roche, 1096176)/PBS. Following three times washing in PBS for 10 min each at RT,
162 specimens were incubated for 1.5 hr at RT with 1:500 anti-rabbit IgG(H+L)-Alexa 488-
163 conjugated antibody (Donkey; Invitrogen, A21206), anti-mouse IgG_{2a}-Alexa 568-
164 conjugated antibody (Goat; Invitrogen, A21134), anti-rat IgG (H+L)-Alexa 488-
165 conjugated antibody (Goat; Invitrogen, A11006) and 1:2000 DAPI. After washing three
166 times in PBS for 10 min at RT, fluorescent images were obtained using the Nikon A1R
167 confocal microscope.
168
169 **Plasmids**
170 pAAV-hSynapsin1-GCaMP6s-P2A-mRuby3 was purchased from Addgene
171 (112007). Full-length cDNA of GCaMP6s was PCR-amplified:
172 forward 5'- GCGTACCACTGTGGCATCGATGCCACCATGGGTTCTCA -3',
173 reverse 5'- GCCCGTACATCGCATCGATTTACTTGTACAGCTCGT -3'.
174 The retroviral vector RCAS-EGFP was digested with ClaI to remove EGFP, into which
175 a DNA fragment was inserted by In-Fusion HD Cloning Kit (TAKARA) to produce
176 RCAS-GCaMP6s-P2A-mRuby3. RCAS-GapEGFP is as previously described (Murai et
177 al., 2015)
178
179 **Preparation of retroviral vector particles**
180 RCAS-GCaMP6s-P2A-mRuby3 was transfected into the chicken fibroblast line
181 cells DF1 using Lipofectamin 2000 (Invitrogen). Transfected cells were cultured in 10
182 cm culture dish until confluent. The supernatant of transfected DF1 was collected for viral
183 precipitation, from which retroviral particles were prepared using Retro-Concentin™
184 Virus Precipitation Solution (SBI, RV100A-1).
185
186 **Intracellular Ca^{2+} imaging in the gut contractile organoid**
187 At day 2 or day 3 of cell culture, 10 mg/ml polybrene solution (final
188 concentration 4 µg/ml, Nacalai, 12996-81) and 20 µl opti-mem with above mentioned
189 virus particles were added to the culture medium to transfect GCaMP6s into organoid-
190 forming cells. The medium was replaced with fresh medium at day 5 and Ca^{2+} imaging
191 was performed at day 7. Time-lapse images were obtained using the confocal microscope
192 (Nikon, A1R) with 700 or 450 msec intervals, and exported intensity of each region of

193 interest (ROI) into an excel file by time measurement (Nikon, NIS-Elements). From the
194 excel file, the graphs were plotted with the fluorescence intensity by setting the beginning
195 of the measurement to zero.
196
197 **Drug administration**
198 Carbenoxolone (CBX; nacalai tesque, 32775-51) /H_2O, 18beta-Glycyrrhetinic
199 acid (18β-GA; abcam, ab142579)/DMSO and (-)-Blebbistatin (FUJIFILM Wako, 021-
200 17041) were prepared. Time-lapse images were acquired for a single organoid before and
201 after the drug administration. Following the drug adding, organoids were allowed to rest
202 for 30 min to avoid possible effect of turbulence of the medium, and time-lapse images
203 were taken for 5 min.
204
205 **Three-well hydrogel fabrication**
206 The photoinitiator P2CK was synthesized as previously reported (Li et al., 2013).
207 The target product was verified using proton NMR and Bruker's TopSpin software.
208 Gelatin-Norbornene was synthesized based on previous report (Van Hoorick et al., 2018).
209 The final reaction mixture was transferred to a dialysis tube (5-6 kDa; Spectra Por, cat.
210 no. 132680T) for dialysis against pure water at 40°C for 3 days. After dialysis, the
211 solution's pH was carefully adjusted to 8.0.
212 A piece of 3-well hydrogel was fabricated on a glass bottom dish (Matsunami)
213 from 100 μL of a solution containing 20 wt % Gelatin-Norbornene, 2 mM of the
214 photoinitiator P2CK, and 20 mM of crosslinker (DTT) (TCI, #D1071) using a two-photon
215 microscope with controllable laser power in 3D space according to the voxel file input
216 (Olympus, in house customized). The voxel files specifying the 3D shape of the hydrogel
217 were designed with Fusion 360 software. (Autodisk).
218
219
220 **Results**
221 **Spheroids were formed from muscle layer-derived cells of the embryonic hindgut**
222 To develop a culture condition that would facilitate analyses of gut motility, we
223 dissected the muscle layer (also called *tunica muscularis*) from the hindgut of E15
224 embryos by removing the serosa and intestinal epithelium (mucosa) (Fig. S1). The
225 isolated muscle layer was dissociated into single cells to prepare 5.0×10^5 cells per culture
226 dish. We started analyses with a culture condition with FBS-free medium and Matrigel
227 as substrate as previously described for cultures in mice of gastrointestinal cells including
228 serosa (Wang et al., 2018). We tested three kinds of FBS-free media: DMEM/Ham's F-

229 12, Ham's F-12, and Neurobasal media (see Materials and Methods). When cultured in
230 DMEM/Ham's F-12 or Ham's F-12, dissociated cells formed very small aggregates
231 containing several cells at day 1, the morphology of which did not change significantly
232 until day 5 (Fig. 1A). In clear contrast, when cultured in the Neurobasal medium, cells
233 formed clusters that were interconnected by elongated cells with neighboring clusters as
234 early as day 1. These clusters grew as larger aggregates by day 3, and became spherical
235 by day 5. Such spheroids were not observed in the conditions with Ham's F-12 or
236 DMEM/Ham's F-12. We also tested different substrates, Poly-Lysine or collagen for dish
237 coating with the Neurobasal medium, but neither one yielded spheroid. To know how the
238 spherical aggregates were formed under the condition of Neurobasal medium and
239 Matrigel, we took time-lapse images at two-hour intervals. Originally sparse clusters that
240 were loosely connected by extended cells merged each other forming progressively larger
241 clusters (Fig. 1B, Movie 1). In the following experiments, we focused on the spheroids
242 formed under the condition of Neurobasal medium and Matrigel coating.
243
244 **The gut muscle layer-derived spheroids displayed periodic contractions**
245 The spheroids underwent reiterative contractions at day 3, and these contractions
246 were observed at least until day 7 of culture (Fig. 2A, Movie 2). Time-lapse imaging of
247 the contractions combined with quantitative assessments by ImageJ (see Materials and
248 Methods) showed that the average frequencies of contractions in each cluster/spheroid
249 at day 3, day 5, and day 7, were 3.32, 3.04, and 2.97 contractions/min, respectively (Fig.
250 2B), which largely corresponded to the rhythm of the E16 chicken embryonic intact gut
251 (Chevalier et al., 2019).
252
253 **The contracting spheroid was composed of ICCs and SMCs**
254 To determine the cell types comprising the spheroids, we performed
255 immunostaining with antibodies for the chicken c-Kit protein (for ICCs; Yagasaki et al.,
256 2022) and αSMA (for SMCs). It is known that ICCs and SMCs are derived from common
257 progenitors which are c-Kit$^+$/αSMA$^+$, and that after differentiation ICCs and SMCs are c-
258 Kit$^+$/αSMA$^-$ and c-Kit$^-$ /αSMA$^+$, respectively (Duband et al., 1993, Kluppel et al., 1998).
259 In the clusters at day 3, c-Kit$^+$/αSMA$^-$ signals were detected in the internal region, and c-
260 Kit$^+$/αSMA$^+$ signals at the periphery (Fig. 3A, Day 3), suggesting that internal cells were
261 differentiated ICCs, whereas peripheral cells were ICC/SMC progenitors. At day 5
262 onward, c-Kit$^+$/αSMA$^-$ cells and c-Kit$^-$/αSMA$^+$ cells were segregated which were located
263 internally and peripherally, respectively (Fig. 3A, Day 5), and this spatial segregation of
264 the cells remained unchanged until day 7 (Fig. 3A, Day 7), the latest stage examined in

265 this study. Infection of RCAS-GapEGFP into a forming spheroid further visualized
266 multipolar ICCs in the internal region (Fig. 3B), known to be characteristic of ICC-MY
267 which would normally reside in the layer of myenteric plexus (Mei et al., 2009, Sanders
268 et al., 2014). ICCs of a different type were also recognized, which were elongated, thin,
269 and lining underneath the peripheral SMCs (Fig. 3A, Day 7). It is possible that they were
270 ICC-IM, known to be embedded in and tightly associated with smooth muscles in the gut
271 (Iino and Horiguchi, 2006, Huizinga et al., 2011). Unexpectedly, the spheroid contained
272 few neural cells (ENS), if any, revealed by anti-Tuj1 antibody (Fig. S2).
273 Since ICCs and SMCs were spatially segregated in the sphenoid, we stained with
274 anti N-cadherin antibody (E-cadherin is positive solely in the mucosa/endoderm)
275 (Graham et al., 2017, Grosse et al., 2011). N-cadherin signals were seen in the internal
276 ICCs, and not in the peripheral SMCs (Fig. 3C). Thus, it is likely that N-cadherin plays a
277 role in the segregation.
278 In summary, the hindgut-derived spheroid displays three prominent
279 characteristics: (1) a dominant occupation by ICCs and SMCs with neglectable
280 contribution by ENS, (2) self-organization ability of internal ICCs encapsuled by a thin
281 layer of SMCs, (3) contractions with periodic rhythm. Based on these characteristics, we
282 designated this spheroid as "gut contractile organoid".
283
284 **Contraction-associated intracellular Ca^{2+} transients were coordinated between**
285 **ICCs and SMCs in the gut contractile organoid**
286 It has been reported that Ca^{2+} dynamics are important for pacemaker activity in
287 ICCs and contractions of SMCs. Ca^{2+} flows into ICCs via voltage-dependent Ca^{2+}
288 channels and propagates to SMCs, causing the gut muscle contractions (Baker et al.,
289 2021). We therefore investigated the Ca^{2+} dynamics in our gut contractile organoids.
290 Organoid-forming cells were infected with a RCAS-vector encoding GCaMP6s, a Ca^{2+}
291 indicator that emits EGFP fluorescence in response to Ca^{2+} influx, and mRuby3 as a
292 reporter (Fig. 4A). GCaMP6s-organoids were subjected to time-lapse imaging analyses
293 by confocal microscopy. As expected, the oscillations rhythm of Ca^{2+} transients as a
294 whole organoid was concomitant with that of contractions (Fig. 4B, Movie 4).
295 Taking advantage of the spatial segregation between ICCs (internal) and SMCs
296 (peripheral) (Fig. 3A), we compared the Ca^{2+} oscillation rhythm among ICCs and SMCs
297 (homotypically) and between ICC-SMC (heterotypically). We set up 3 regions of interests
298 (ROIs) in the central region, with one ROI corresponding to one cell, and captured the
299 Ca^{2+} transients. The three ROIs exhibited a synchronous pattern of Ca^{2+} oscillations (Fig.
300 4C, ICCs). Similarly, Ca^{2+} oscillations in three ROIs in the SMC layer were synchronous

301 (Fig. 4C, SMCs). These data highlight active communications taking place intercellularly
302 within ICCs and SMCs, respectively. We further compared Ca^{2+} oscillations between
303 ICC-SMC. Setting up with one ROI in an ICC, and one in a SMC. Again, the Ca^{2+} rhythm
304 was synchronized between these heterotypic cell types (Fig. 4C, ICC/SMC). With a closer
305 look, a rise of the Ca^{2+} transient in the ICC preceded that in SMC with a time lag (also
306 called latency) of 690 msec in average (Fig. 4C, ICC/SMC), suggestive of a propagation
307 of Ca^{2+} signals from ICC to SMC consistent with previous reports (Baker et al., 2021).
308

309 **Gap junction plays a role in ICC-to-SMC signaling**

310 Although a series of gut motility studies have proposed an importance of gap
311 junctions, rigid evidence has been limited due to a lack of experimental model. Our gut
312 contractile organoid should prove useful for clarifying the roles of gap junctions in the
313 synchronous motility, since intercellular synchronization was observed between/among
314 identifiable cells (ICCs and SMCs) as shown above. We performed pharmacological
315 assessments using gap junction inhibitors including carbenoxolone (CBX) and 18β-
316 glycyrrhetinic acid (18β-GA; Chevalier, 2018, Takeda et al., 2005), two of the most
317 widely used pharmacological inhibitors used to study gap junctions.

318 Following inhibitor administration into day 7 culture medium, organoids were
319 allowed to rest for 30 min to exclude possible effects by the administration, for example,
320 turbulence of the medium. With CBX or 18β-GA in the culture medium, the periodic
321 contraction of an organoid was retained with almost the same frequency as the control
322 (Fig. S3, Movie 3). We then examined whether the intercellular
323 synchronization/coordination was affected by the inhibitors. Similarly to Fig. 4, three
324 ROIs were set either in ICCs or SMCs territories for assessment of Ca^{2+} transients. The
325 same cells in a single organoid were tracked for their Ca^{2+} transients before and after the
326 inhibitor administration. Contrary to our expectation, none of 10 μM, 20 μM and 100 μM
327 concentrations of these inhibitors showed detectable inhibition of the synchronous
328 patterns of Ca^{2+} transients (Fig. 5A, B show 100 μM of CBX, Movie 5).

329 In contrast, when an ICC and SMC were compared, the preceding rise of Ca^{2+}
330 transient in ICC was abolished, although overall synchronization was retained between
331 these the cells (Fig. 5C). Collectively, while the contribution by gap junction to the
332 periodic contraction and intercellular synchronization in the organoid is relatively limited,
333 the ICC-to-SMC signals require gap junction-mediated communications, at least partly.
334

335 **Blebbistatin abolished organoidal contractions and oscillatory patterns of Ca^{2+}**
336 **transients**

337 Toward searching for factors that regulate the coordination between/among ICCs
338 and SMCs, we tested blebbistatin, a specific inhibitor of myosin II, which was expected
339 to cease organoidal contractions. Experimental procedures were similar to those for gap
340 junction inhibitors. We found that blebbistatin ceased periodic contractions of organoids
341 in a concentration-dependent manner, with 10 μM ceasing it completely (Fig. 6A, Movie
342 6). We examined Ca^{2+} transients in these contraction-inhibited organoids. Markedly,
343 periodic Ca^{2+} transients not only in SMCs, but also in ICCs were extinguished, resulting
344 in no/little synchronous Ca^{2+} patterns among and between ICCs and SMCs (Fig. 6B-E).
345 Although the possibility is not excluded that blebbistain directly inhibited non-muscle
346 myosin II in ICCs, these findings imply that the contractility feeds back to ICCs to
347 generate their periodic rhythm.
348
349 **Inter-organoidal coordination was mediated by SMCs**
350 During analyses with our novel organoids, we found that they easily fuse to each
351 other, suggesting that organoids grow by progressive fusion (Fig. 7A, Movie 7). This also
352 raised the possibility that the synchronous Ca^{2+} transients among organoid-constituting
353 cells (Fig. 4C) might be a consequence of phasic coordination upon the fusion of multiple
354 organoids that had shown different oscillatory phases. To test this possibility, we
355 transferred two organoids in a petri dish, and allowed them to fuse. Before the fusion,
356 Ca^{2+} oscillatory rhythm was indeed out of phase in the two organoids (Fig. 7B, Movie 8).
357 Markedly, upon fusion by 24 hours, their rhythm became in phase/synchronous (Fig. 7B,
358 Movie 8).
359 Since we noticed that cellular protrusions were often observed around the time of
360 organoidal fusion, we reasoned that these cellular processes would mediate the fusion and
361 its subsequent synchronization of Ca^{2+} transients (Fig. 7C). To test this, we developed a
362 3-well hydrogel with narrow channels connecting the wells (Fig. 8A). Organoids were
363 placed separately in each well, which prevented the fusion of organoidal bodies, but
364 allowed extension of cellular processes through the narrow channels and contact with
365 each other (Fig. 8B). After 72 hours of placement of organoids, cellular processes as well
366 as several cell bodies were present within the channel, and Ca^{2+} transients became
367 synchronized among the three organoids (Fig. 8C, Movie 9). However, with careful
368 examination, we also noticed that organoid-derived cells crawled out from the wells to
369 cover the top surface of the hydrogel, connecting the three organoids (Fig. 8D). Thus,
370 another possibility was raised that these crawled out cells would mediate the inter-
371 organoidal synchronization.
372 To test this possibility, we prepared a 3-well hydrogel in which the three wells

were disconnected (no channels) so that organoid-derived cellular processes were not able to connect each other (Fig. 8E). By 3 days of culture, the top surface of the hydrogel was indeed covered by cells in a similar way to Fig. 8D. These cells were positive for αSMA but negative for c-Kit (Fig. 8F), indicating that they were SMCs that were somehow detached and crawled out from the peripheral layer of the organoids. Importantly, coincided with the top-coverage by the SMCs, the three organoids in the disconnected wells displayed synchronized Ca^{2+} transients, highlighting the role of SMCs in mediating coordination between organoids (Fig. 8G, Movie 10). Gap junction inhibitor yielded no/little effects on the Ca^{2+} transient coordination (Fig. 8H, Movie 11).

Discussion

We have developed a novel gut contractile organoid, which displays several unique characteristics: 1) it undergoes periodic contractions, 2) differentiation states of ICCs (c-Kit^{+}/αSMA^{-}) and SMCs (c-Kit^{-}/αSMA^{+}) are maintained at least until day 7 in the organoid, 3) the organoid is composed essentially of two types of cells, ICCs and SMCs, with few ENS cells, if any, 4) ICCs (internal) and SMCs (peripheral) can be distinguished for their localization in a living organoid, allowing 5) GCaMP-visualization of Ca^{2+} transients and assessments of cell interactions between and among ICCs and SMCs. These characteristics circumvent, at least partly, obstacles that have hampered analyses in the research of gut peristalsis, such as unstable differentiation state of ICCs and SMCs in cultures, and difficulties in identifying these cells in living preparations. In studies of gut movements, how ICCs generate/maintain their periodic rhythm and how ICCs and SMCs interact with each other have been long-standing questions, and our organoids offer powerful advantages to address these and to understand the cellular mechanisms underlying the gut contractions/peristaltic motility.

Contrasting with many cases in organoid studies that have aimed at a *maximum* recapitulation of the intact organ, our gut contractile organoid is composed of a (probably) *minimum* number of cell types that suffice the generation and/or maintenance of rhythmic contractions, allowing high-resolution analyses at the cellular level. For example, adding ENS components to our organoid would allow the clarification of the role of ENS in the gut contraction. While the majority of internal cells in the organoid are ICCs (c-Kit^{+}/αSMA^{-}), the possibility cannot be excluded that platelet-derived growth factor receptor-α positive (PDFGRα^{+}/c-Kit^{-}/αSMA^{-}) cells, another type of interstitial cells (fibroblast-like cell) known to mediate neural activity to SMCs in the mouse gut (Sanders

408 et al., 2024, Sanders et al., 2016), are included in our organoid. Available antibody against
409 the chicken PDFGRα protein is awaited.
410
411 **Coordinated Ca^{2+} transients in ICC/SMC populations in the gut contractile**
412 **organoid**
413 Measurement and quantification analyses with ICCs and SMCs that are
414 identifiable in the living organoid revealed exquisite coordination of Ca^{2+}
415 transients/oscillation homotypically between ICC-ICC and SMC-SMC and
416 heterotypically between SMC-ICC (Fig. 4C). Notably, a rise (upstroke) of Ca^{2+} transient
417 in ICCs precedes that of SMCs with a time lag (also called latency) of 690 msec,
418 suggesting a directed signaling from ICC to SMC. These observations are consistent with
419 previous studies using ICC- and SMC-specific transgenic mice that expressed GCaMP
420 and RCaMP, respectively (Baker et al., 2021). In that study, the authors assessed Ca^{2+}
421 transients in submucosal ICCs (ICC-SM) and compared them with those in their adjacent
422 circular muscles, and showed that the rise of GCaMP signal preceded that of RCaMP with
423 a latency of 56 +/- 14 msec. With these observations, they concluded that ICC-SM signals
424 to its adjacent SMCs. In our study, time-lapse imaging was mostly performed with 700
425 msec intervals. Further studies with shorter intervals are awaited to know the latency time
426 would be shorter than 690 msec in average.
427
428 **Contribution of gap junction to ICC-to-SMC signaling**
429 Effects by the block of gap junction by CBX or 18β-GA were relatively limited
430 in our organoid assays: synchronous patterns of Ca^{2+} transients remained unchanged
431 between SMC-SMC and ICC-ICC. In contrast, signaling from ICCs to SMCs was
432 specifically affected by these inhibitors, in which the preceding rise of Ca^{2+} transient in
433 ICCs was abolished. The contribution of gap junction to the ICC-to-SMC signaling was
434 previously reported in mouse gut, which was from intramuscular ICCs (ICC-IM) to their
435 adjacent circular smooth muscles. However, interpretation of the role of gap junction in
436 ICC-SMC interactions, in general, has been under big debate. Some studies reported that
437 CBX or 18β-GA failed to inhibit these interactions or peristaltic motilities (Komuro et al.,
438 1996, Rohr et al., 1998, Schultz et al., 2003), or that electron microscopy did not detect
439 structures of gap junction in longitudinal muscles (Cousins et al., 2003, Daniel and Wang,
440 1999, Gabella and Blundell, 1981). Contribution of gap junctions to the gut motility
441 appears to be highly variable in different regions of gastrointestinal tract, for example,
442 stomach versus colon (Iino et al., 2007, Yang et al., 2012) . And a detection of gap
443 junction structures or mRNA/protein of Connexins (Cx; a component of gap junction)

444 does not necessarily mean that the gap junction is functional. Dominant negative form of
445 gap junction might be useful. Currently, ICC- or SMC-specific gene manipulations in our
446 organoid are not available, and further studies are awaited. It is intriguing that the
447 coordination between SMC-SMC and ICC-ICC was unaffected by the inhibitors in our
448 organoids. The possibility cannot be excluded that gap junctions that are not inhibited by
449 CBX or 18β-GA might operate. However, since these two inhibitors have popularly been
450 used to block a wide range of gap junctions, alternative possibility arises that cell
451 communications particularly between SMC-SMC are mediated by other mechanisms than
452 gap junctions, including mechanical signals as recently shown for coordinated Ca^{2+}
453 signaling in cardiac muscle cells (Fukui et al., 2021).
454
455 **Possible feedback from SMC's contractility to ICC's oscillatory rhythm**
456 Blebbistatin prevented the contraction of the organoids, which was concomitant
457 with abrogation of Ca^{2+} transients in ICCs. Since it has been reported that thick myosin
458 fibers necessary for the contraction are found only in SMCs but not in ICCs
459 (Gherghiceanu and Popescu, 2005, Rumessen and Thuneberg, 1996, Rumessen and
460 Thuneberg, 1991, Sun et al., 2006), it is likely that ICCs do not have contractile ability.
461 Our observations therefore promote the possibilities that ICC's pace-making activity
462 requires its own non-muscle myosin II, and/or mechanical feedback by contracting SMCs.
463 Currently, techniques that distinguish between these possibilities are unavailable.
464 Nevertheless, if it is the latter case, it would indicate a signaling from SMC to ICC, the
465 direction of which is unprecedented, since previous literatures had shown that it was
466 solely an ICC-to-SMC signaling process that dictated the rhythm of SMC's contraction.
467 We presume that the SMC's contribution to ICC's pace-making is highly possible since
468 this notion is further supported by other findings obtained in this study showing that
469 SMCs mediate inter-organoidal phase coordination (Fig. 8) as more discussed below.
470 It is of note that the reciprocal interactions between pace-making cells and their
471 effectors have been reported in studies of neural circuit establishment. Spontaneous
472 activities emerging in motor neurons during embryogenesis are regulated by feedback
473 from their governing muscle's contractions so that motor neurons get organized to display
474 coordinated and stable oscillatory activities (Zeng et al., 2021). Thus, it is tempting to
475 speculate that during early gut peristalsis, ICCs might receive feedback from their
476 governing SMCs to generate more stable coordination of pace-making activity among
477 ICCs. Indeed, we have previously reported that in the very early embryonic gut, origins
478 of peristaltic wave (OPW) are randomly distributed along the gut axis, but they later

479 become confined to specific sites showing that ICCs undergo more stable and coordinated
480 pace-making (Shikaya et al., 2022).
481
482 **Interactions between ICCs and SMCs in the gut contractile organoid**
483 The organoid developed in this study was derived from the muscle layer (also
484 called *tunica muscularis*) of chicken E15 hindgut devoid of mucosa and serosa, in which
485 myenteric ICCs (ICC-MY), intramuscular ICCs (ICC-IM), and submucosal ICCs (ICC-
486 SM) are localized in a way similar to those in mice, shown by staining with antibody
487 against the chicken c-Kit protein (Yagasaki et al., 2022). In the current study, c-Kit
488 antibody-staining showed two types of cells in morphology in the gut contractile
489 organoid: one is multipolar and N-cad-positive ICCs located centrally, and the other is
490 ICCs that are thin in shape, N-cad negative, and lining beneath the most external layer of
491 SMCs. Based on the knowledge obtained in studies with mammalian species that ICC-
492 MY are multipolar whereas ICC-IM are bipolar and tightly associated with adjacent
493 SMCs (Huizinga et al., 2011, Iino and Horiguchi, 2006), it is conceivable in our organoids
494 that the central cells are ICC-MY, and the peripherally lining ones are ICC-IM. In
495 addition, it has been reported in mice that signaling from ICC-IM to SMCs is gap
496 junction-dependent. Collectively, our observations that gap junction-dependent signal
497 found between ICCs (central ICC) and SMCs in the organoid (Fig. 5C) could be
498 interpreted as follows: ICC-MY (central) signals to ICC-IM (second-most peripheral),
499 which in turn signals to the external SMCs mediated partly by gap junction. Such
500 sequences of signaling (ICC-MY to ICC-IM to SMCs) has also been proposed in the
501 intact gut in mammals, although rigid evidence has not been known. Direct comparison
502 of Ca^{2+} transients between the ICC-IM-like cells and SMCs in our organoid was
503 technically very difficult since these two cells were both thin and tightly associated each
504 other.
505
506 **The gut contractile organoid provides a useful model and tool for studying phasic**
507 **coordination of oscillatory rhythm**
508 To understand the gut peristaltic movements, which reiterate at specific sites
509 along the gut axis (Shikaya et al., 2022), deciphering the mechanisms underlying the
510 coordination/synchronization of oscillators among multiple cells is critical. Exploiting the
511 finding obtained in the current study that multiple organoids easily fuse each other in vitro,
512 we have found that two organoids with different oscillatory rhythm eventually coordinate
513 their phases upon the fusion (Fig. 7). This suggests the ability of ICCs to adjust their
514 rhythm to their neighbors. During identification of the rhythm-adjustment mediators

using the 3-well hydrogel, contrasting with our original expectation, SMCs that were crawled out from the organoids and covered the top surface of the hydrogel were able to mediate the rhythm coordination among organoids (Fig. 8). Whether cellular thin protrusions connected with each other in narrow channels mediate the coordination remains undetermined. Nevertheless, our findings have revealed a novel role of SMCs in mediating rhythm coordination, and as discussed above, this supports the notion of a SMC-to-ICC signaling. It is unlikely that gap junction plays a major role in such signaling since gap junction inhibitor yielded no detectable effects in the assays using the 3-well hydrogel.

In summary, the gut contractile organoid developed in this study serves as a powerful model to study the establishment and maintenance of oscillatory rhythm (pace-making) and their coordination in the multicellular systems.

Acknowledgement

We thank Dr. Scott Gilbert for careful reading of the manuscript and discussion. We also thank National BioResource Project (Chicken-Quail, Nagoya University) for their technical help. This work was supported by JSPS KAKENHI Grant Numbers; 23H04933, 20H03259, 20K20520, 20K21425 for Y. T., and 21K06198, 23H04702 for M. I., and FY 2022 Kusunoki 125 of Kyoto University 125th Anniversary Fund for M. I., and Ginpu Funds (Kyoto University) and incu-be fund (Leave a Nest Co., Ltd.) for R. Y.. R. Y. is an ex-fellow of JSPS.

References

Baker, S. A., Leigh, W. A., Del Valle, G., De Yturriaga, I. F., Ward, S. M., Cobine, C. A., Drumm, B. T. and Sanders, K. M. (2021) 'Ca(2+) signaling driving pacemaker activity in submucosal interstitial cells of Cajal in the murine colon', Elife, 10. DOI: 10.7554/eLife.64099.

Barajas-Lopez, C., Berezin, I., Daniel, E. E. and Huizinga, J. D. (1989) 'Pacemaker activity recorded in interstitial cells of Cajal of the gastrointestinal tract', Am J Physiol, 257(4 Pt 1), pp. C830-5. DOI: 10.1152/ajpcell.1989.257.4.C830.

Camborova, P., Hubka, P., Sulkova, I. and Hulin, I. (2003) 'The pacemaker activity of interstitial cells of Cajal and gastric electrical activity', Physiol Res, 52(3), pp. 275-84. Available at: https://www.ncbi.nlm.nih.gov/pubmed/12790758.

Chevalier, N. R. (2018) 'The first digestive movements in the embryo are mediated by mechanosensitive smooth muscle calcium waves', Philos Trans R Soc Lond B Biol Sci, 373(1759). DOI: 10.1098/rstb.2017.0322.

551 Chevalier, N. R., Ammouche, Y., Gomis, A., Teyssaire, C., de Santa Barbara, P. and Faure, S. (2020)
552 'Shifting into high gear: how interstitial cells of Cajal change the motility pattern of the developing
553 intestine', Am J Physiol Gastrointest Liver Physiol, 319(4), pp. G519-g528. DOI:
554 10.1152/ajpgi.00112.2020.
555 Chevalier, N. R., Dacher, N., Jacques, C., Langlois, L., Guedj, C. and Faklaris, O. (2019) 'Embryogenesis
556 of the peristaltic reflex', J Physiol, 597(10), pp. 2785-2801. DOI: 10.1113/jp277746.
557 Cousins, H. M., Edwards, F. R., Hickey, H., Hill, C. E. and Hirst, G. D. (2003) 'Electrical coupling between
558 the myenteric interstitial cells of Cajal and adjacent muscle layers in the guinea-pig gastric antrum',
559 J Physiol, 550(Pt 3), pp. 829-44. DOI: 10.1113/jphysiol.2003.042176.
560 Daniel, E. E. and Wang, Y. F. (1999) 'Gap junctions in intestinal smooth muscle and interstitial cells of
561 Cajal', Microsc Res Tech, 47(5), pp. 309-20. DOI: 10.1002/(SICI)1097-
562 0029(19991201)47:5<309::AID-JEMT2>3.0.CO;2-K.
563 Duband, J. L., Gimona, M., Scatena, M., Sartore, S. and Small, J. V. (1993) 'Calponin and SM 22 as
564 differentiation markers of smooth muscle: spatiotemporal distribution during avian embryonic
565 development', Differentiation, 55(1), pp. 1-11. DOI: 10.1111/j.1432-0436.1993.tb00027.x.
566 Fukui, H., Chow, R. W., Xie, J., Foo, Y. Y., Yap, C. H., Minc, N., Mochizuki, N. and Vermot, J. (2021)
567 'Bioelectric signaling and the control of cardiac cell identity in response to mechanical forces',
568 Science, 374(6565), pp. 351-354. DOI: 10.1126/science.abc6229.
569 Gabella, G. and Blundell, D. (1981) 'Gap junctions of the muscles of the small and large intestine', Cell
570 Tissue Res, 219(3), pp. 469-88. DOI: 10.1007/BF00209987.
571 Gherghiceanu, M. and Popescu, L. M. (2005) 'Interstitial Cajal-like cells (ICLC) in human resting
572 mammary gland stroma. Transmission electron microscope (TEM) identification', J Cell Mol Med,
573 9(4), pp. 893-910. DOI: 10.1111/j.1582-4934.2005.tb00387.x.
574 Graham, H. K., Maina, I., Goldstein, A. M. and Nagy, N. (2017) 'Intestinal smooth muscle is required for
575 patterning the enteric nervous system', J Anat, 230(4), pp. 567-574. DOI: 10.1111/joa.12583.
576 Grosse, A. S., Pressprich, M. F., Curley, L. B., Hamilton, K. L., Margolis, B., Hildebrand, J. D. and
577 Gumucio, D. L. (2011) 'Cell dynamics in fetal intestinal epithelium: implications for intestinal
578 growth and morphogenesis', Development, 138(20), pp. 4423-32. DOI: 10.1242/dev.065789.
579 Huizinga, J. D., Martz, S., Gil, V., Wang, X. Y., Jimenez, M. and Parsons, S. (2011) 'Two independent
580 networks of interstitial cells of cajal work cooperatively with the enteric nervous system to create
581 colonic motor patterns', Front Neurosci, 5, pp. 93. DOI: 10.3389/fnins.2011.00093.
582 Huizinga, J. D., Thuneberg, L., Kluppel, M., Malysz, J., Mikkelsen, H. B. and Bernstein, A. (1995) 'W/kit
583 gene required for interstitial cells of Cajal and for intestinal pacemaker activity', Nature, 373(6512),
584 pp. 347-9. DOI: 10.1038/373347a0.
585 Iino, S. and Horiguchi, K. (2006) 'Interstitial cells of cajal are involved in neurotransmission in the
586 gastrointestinal tract', Acta Histochem Cytochem, 39(6), pp. 145-53. DOI: 10.1267/ahc.06023.

587 Iino, S., Horiguchi, S., Horiguchi, K. and Nojyo, Y. (2007) 'Interstitial cells of Cajal in the gastrointestinal
588 musculature of W mutant mice', Arch Histol Cytol, 70(3), pp. 163-73. DOI: 10.1679/aohc.70.163.
589 Kito, Y., Ward, S. M. and Sanders, K. M. (2005) 'Pacemaker potentials generated by interstitial cells of
590 Cajal in the murine intestine', Am J Physiol Cell Physiol, 288(3), pp. C710-20. DOI:
591 10.1152/ajpcell.00361.2004.
592 Kluppel, M., Huizinga, J. D., Malysz, J. and Bernstein, A. (1998) 'Developmental origin and Kit-dependent
593 development of the interstitial cells of cajal in the mammalian small intestine', Dev Dyn, 211(1),
594 pp. 60-71. DOI: 10.1002/(SICI)1097-0177(199801)211:1<60::AID-AJA6>3.0.CO;2-5.
595 Komuro, T., Tokui, K. and Zhou, D. S. (1996) 'Identification of the interstitial cells of Cajal', Histol
596 Histopathol, 11(3), pp. 769-86. Available at: https://www.ncbi.nlm.nih.gov/pubmed/8839765.
597 Li, Z. Q., Torgersen, J., Ajami, A., Mühleder, S., Qin, X. H., Husinsky, W., Holnthoner, W., Ovsianikov,
598 A., Stampfl, J. and Liska, R. (2013) 'Initiation efficiency and cytotoxicity of novel water-soluble
599 two-photon photoinitiators for direct 3D microfabrication of hydrogels', Rsc Advances, 3(36), pp.
600 15939-15946. DOI: 10.1039/c3ra42918k.
601 Liu, L. W., Thuneberg, L. and Huizinga, J. D. (1998) 'Development of pacemaker activity and interstitial
602 cells of Cajal in the neonatal mouse small intestine', Dev Dyn, 213(3), pp. 271-82. DOI:
603 10.1002/(SICI)1097-0177(199811)213:3<271::AID-AJA4>3.0.CO;2-R.
604 Mei, F., Han, J., Huang, Y., Jiang, Z. Y., Xiong, C. J. and Zhou, D. S. (2009) 'Plasticity of interstitial cells
605 of cajal: a study in the small intestine of adult Guinea pigs', Anat Rec (Hoboken), 292(7), pp. 985-
606 93. DOI: 10.1002/ar.20928.
607 Murai, H., Tadokoro, R., Sakai, K. and Takahashi, Y. (2015) 'In ovo gene manipulation of melanocytes and
608 their adjacent keratinocytes during skin pigmentation of chicken embryos', Dev Growth Differ,
609 57(3), pp. 232-41. DOI: 10.1111/dgd.12201.
610 Rohr, S., Kucera, J. P. and Kleber, A. G. (1998) 'Slow conduction in cardiac tissue, I: effects of a reduction
611 of excitability versus a reduction of electrical coupling on microconduction', Circ Res, 83(8), pp.
612 781-94. DOI: 10.1161/01.res.83.8.781.
613 Rumessen, J. J. and Thuneberg, L. (1991) 'Interstitial cells of Cajal in human small intestine. Ultrastructural
614 identification and organization between the main smooth muscle layers', Gastroenterology, 100(5
615 Pt 1), pp. 1417-31. Available at: https://www.ncbi.nlm.nih.gov/pubmed/2013387.
616 Rumessen, J. J. and Thuneberg, L. (1996) 'Pacemaker cells in the gastrointestinal tract: interstitial cells of
617 Cajal', Scand J Gastroenterol Suppl, 216, pp. 82-94. DOI: 10.3109/00365529609094564.
618 Sanders, K. M., Drumm, B. T., Cobine, C. A. and Baker, S. A. (2024) 'Ca(2+) dynamics in interstitial cells:
619 foundational mechanisms for the motor patterns in the gastrointestinal tract', Physiol Rev, 104(1),
620 pp. 329-398. DOI: 10.1152/physrev.00036.2022.
621 Sanders, K. M., Kito, Y., Hwang, S. J. and Ward, S. M. (2016) 'Regulation of Gastrointestinal Smooth
622 Muscle Function by Interstitial Cells', Physiology (Bethesda), 31(5), pp. 316-26. DOI:

10.1152/physiol.00006.2016.

Sanders, K. M., Publicover, N. G. and Ward, S. M. (1991) 'Involvement of interstitial cells of Cajal in pacemaker activity of canine colon', J Smooth Muscle Res, 27(1), pp. 1-11. DOI: 10.1540/jsmr.27.1.

Sanders, K. M., Ward, S. M. and Koh, S. D. (2014) 'Interstitial cells: regulators of smooth muscle function', Physiol Rev, 94(3), pp. 859-907. DOI: 10.1152/physrev.00037.2013.

Schultz, T., Daniel, V. and Daniel, E. E. (2003) 'Does ICC pacing require functional gap junctions between ICC and smooth muscle in mouse intestine?', Neurogastroenterol Motil, 15(2), pp. 129-38. DOI: 10.1046/j.1365-2982.2003.00401.x.

Shikaya, Y., Takase, Y., Tadokoro, R., Nakamura, R., Inaba, M. and Takahashi, Y. (2022) 'Distribution Map of Peristaltic Waves in the Chicken Embryonic Gut Reveals Importance of Enteric Nervous System and Inter-Region Cross Talks Along the Gut Axis', Front Cell Dev Biol, 10, pp. 827079. DOI: 10.3389/fcell.2022.827079.

Sun, X., Yu, B., Xu, L., Dong, W. and Luo, H. (2006) 'Interstitial cells of Cajal in the murine gallbladder', Scand J Gastroenterol, 41(10), pp. 1218-26. DOI: 10.1080/00365520600708800.

Takaki, M. (2003) 'Gut pacemaker cells: the interstitial cells of Cajal (ICC)', J Smooth Muscle Res, 39(5), pp. 137-61. DOI: 10.1540/jsmr.39.137.

Takayama, I., Horiguchi, K., Daigo, Y., Mine, T., Fujino, M. A. and Ohno, S. (2002) 'The interstitial cells of Cajal and a gastroenteric pacemaker system', Arch Histol Cytol, 65(1), pp. 1-26. DOI: 10.1679/aohc.65.1.

Takeda, Y., Ward, S. M., Sanders, K. M. and Koh, S. D. (2005) 'Effects of the gap junction blocker glycyrrhetinic acid on gastrointestinal smooth muscle cells', Am J Physiol Gastrointest Liver Physiol, 288(4), pp. G832-41. DOI: 10.1152/ajpgi.00389.2004.

Thomsen, L., Robinson, T. L., Lee, J. C., Farraway, L. A., Hughes, M. J., Andrews, D. W. and Huizinga, J. D. (1998) 'Interstitial cells of Cajal generate a rhythmic pacemaker current', Nat Med, 4(7), pp. 848-51. DOI: 10.1038/nm0798-848.

Torihashi, S., Fujimoto, T., Trost, C. and Nakayama, S. (2002) 'Calcium oscillation linked to pacemaking of interstitial cells of Cajal: requirement of calcium influx and localization of TRP4 in caveolae', J Biol Chem, 277(21), pp. 19191-7. DOI: 10.1074/jbc.M201728200.

Torihashi, S., Nishi, K., Tokutomi, Y., Nishi, T., Ward, S. and Sanders, K. M. (1999) 'Blockade of kit signaling induces transdifferentiation of interstitial cells of cajal to a smooth muscle phenotype', Gastroenterology, 117(1), pp. 140-8. DOI: 10.1016/s0016-5085(99)70560-3.

Van Hoorick, J., Gruber, P., Markovic, M., Rollot, M., Graulus, G. J., Vagenende, M., Tromayer, M., Van Erps, J., Thienpont, H., Martins, J. C., Baudis, S., Ovsianikov, A., Dubruel, P. and Van Vlierberghe, S. (2018) 'Highly Reactive Thiol-Norbornene Photo-Click Hydrogels: Toward Improved Processability', Macromol Rapid Commun, 39(14), pp. e1800181. DOI: 10.1002/marc.201800181.

659 Wang, Q., Wang, K., Solorzano-Vargas, R. S., Lin, P. Y., Walthers, C. M., Thomas, A. L., Martín, M. G.
660 and Dunn, J. C. Y. (2018) 'Bioengineered intestinal muscularis complexes with long-term
661 spontaneous and periodic contractions', PLoS One, 13(5), pp. e0195315. DOI:
662 10.1371/journal.pone.0195315.
663 Yagasaki, R., Shikaya, Y., Kawachi, T., Inaba, M., Takase, Y. and Takahashi, Y. (2022) 'Newly raised anti-
664 c-Kit antibody visualizes morphology of interstitial cells of Cajal in the developing gut of chicken
665 embryos', Dev Growth Differ, 64(8), pp. 446-454. DOI: 10.1111/dgd.12808.
666 Yang, P., Yu, Z., Gandahi, J. A., Bian, X., Wu, L., Liu, Y., Zhang, L., Zhang, Q. and Chen, Q. (2012) 'The
667 identification of c-Kit-positive cells in the intestine of chicken', Poult Sci, 91(9), pp. 2264-9. DOI:
668 10.3382/ps.2011-02076.
669 Zeng, X., Komanome, Y., Kawasaki, T., Inada, K., Jonaitis, J., Pulver, S. R., Kazama, H. and Nose, A.
670 (2021) 'An electrically coupled pioneer circuit enables motor development via proprioceptive
671 feedback in Drosophila embryos', Curr Biol, 31(23), pp. 5327-5340 e5. DOI:
672 10.1016/j.cub.2021.10.005.
673

674

675 **Figure legends**

676 **Figure 1**

677 (A) Culture of muscle layer-derived cells prepared from embryonic hindgut with
678 FBS free-media and substrates. (B) Long-term time-lapse imaging after seeding on
679 Matrigel with Neurobasal media. The images show the ability of these cells to self-
680 assemble at 0, 20, 40, 60, 80 and 100 hours taken from Movie 1. Scale bars: 100 μm in
681 A, B.

682

683 **Figure 2**

684 Forming spheroids in Neurobasal medium and Matrigel exhibited reiterated
685 contractions. (A) Clusters/spheroids on day 3, 5 and 7 exhibited periodic contractions.
686 Graphs show contractions quantified by differences in the intensity of brightfield in
687 sequential images. (B) Frequency of contractions of the cluster/spheroid on day 3-7
688 (N=day 3: 46, day 5: 35, day 7: 60). The number on each graph shows the average of
689 contraction frequencies. Scale bars: 50 μm in A.

690

691 **Figure 3**

692 A cluster/spheroid is composed of ICCs internally and SMCs peripherally. (A)
693 Co-staining with anti-c-Kit- and αSMA antibodies. White arrowheads show co-
694 expression of c-Kit and αSMA at Day 3. Yellow arrowheads indicate a cell expressing
695 αSMA but not c-Kit at day 7. A diagram shows an image of cell arrangement (green: ICC,
696 magenta: SMC) in the spheroid at day 7. (B) Cell morphology in the spheroid at day 6
697 revealed by RCAS-gapEGFP expression. (C) Staining of spheroids at day 5 with anti-N-
698 cadherin antibody. A white arrowhead shows expression of N-cadherin. A yellow
699 arrowhead shows a cell which does not express N-cadherin in the outer region of the
700 spheroid. Scale bars: 30 μm in A-C, 10 μm in a.

701

702 **Figure 4**

703 Ca^{2+} imaging of the gut contractile organoid revealed intercellular
704 synchronization. (A) RCAS-GCaMP6s-P2A-mRuby3 plasmid. (B) Ca^{2+} imaging of gut
705 contractile organoid during relaxation and contraction. Ca^{2+} dynamics (green) and
706 contraction (grey) of gut contractile organoid. (C) Simultaneous measurement of
707 intercellular Ca^{2+} dynamics between ICC-ICC, SMC-SMC or ICC-SMC. Three or two
708 ROIs with Ca^{2+} signal-positive cells were set in a single organoid. Graphs show Ca^{2+}
709 dynamics in the ROIs. Magnified view shows that a rise of Ca^{2+} signal in ICC (green)

710 preceded that in SMC (magenta). Scale bar: 50 μm in B.
711
712 **Figure 5**
713 Gap junction inhibitor exerted limited effects on the synchronization of Ca^{2+}
714 dynamics. GCaMP6s-expressing organoids were cultured with CBX, and three or two
715 ROIs were assessed for their Ca^{2+} synchronization. A single organoid was subjected to
716 the assessment before (0 μM; control) and after administrations of 100 μM CBX. The
717 synchronization was unaffected between (A) SMC-SMC and (B) ICC-ICC, but that in
718 (C) ICC-SMC was partially affected. Magnified view shows that the preceding rise of
719 Ca^{2+} in ICC (green) before CBX was abrogated after CBX. Scale bar: 50 μm in A.
720
721 **Figure 6**
722 The organoidal contraction is important for Ca^{2+} dynamics in ICCs. GCaMP6s-
723 expressing organoids were cultured with Blebbistatin. (A) Ca^{2+} oscillation was
724 extinguished in the entire organoid by administration of Blebbistatin. (B-D) Ca^{2+}
725 dynamics in (B) SMC-SMC, (C) ICC-ICC and (D) ICC-SMC. Three or two ROIs were
726 assessed for their Ca^{2+} synchronization. A single organoid was subjected to the
727 assessment before (0 μM; control) and after administrations of 10 μM Blebbistatin. (E)
728 Ca^{2+} transients in a single ICC in 0 μM, 5 μM, and 10 μM. Scale bar: 50 μm in B.
729
730 **Figure 7**
731 Ca^{2+} dynamics in multiple gut contractile organoids undergo synchronization
732 upon their fusion (A) Time-lapse imaging of organoidal fusion. (B) When two organoids
733 that originally showed independent rhythm of Ca^{2+} fused to each other, their rhythm
734 became synchronized after fusion (24 h). (C) Protrusions between two neighboring
735 organoids. White arrowheads show three protrusions from the left organoid. Scale bars:
736 100 μm in A-C, 20 μm in a.
737
738 **Figure 8**
739 Smooth muscle cells mediate the Ca^{2+} synchronization between organoids (A)
740 Diagram of 3-well hydrogel in which an organoid placed in each well. This gel mold does
741 not allow organoidal bodies to fuse to each other, but allow them to extend/migrate
742 protrusions/cells through a narrow channel connecting the wells (B). (C) After 3 days,
743 three organoids displayed synchronization of Ca^{2+} dynamics. (D) Some organoid-derived
744 cells crawled out from the wells and covered the top surface of the hydrogel, resulting in
745 bridging the three unfused organoids. (E) Diagram of 3-well hydrogel *without* channels

(F) Surface-covering cells were SMCs (αSMA positive and c-Kit-negative). (G) In the hydrogel without channels but with surface-covered SMCs, Ca^{2+} dynamics in the 3 organoids were synchronized. (H) The Ca^{2+} synchronization shown in (G) was not altered by 18β-GA. Scale bars: 50 μm in B, 100 μm in C-H.

Supplementary Figure S1

(A) Chicken embryonic hindgut at E15. The hindgut was dissected from the bottom of the cecum to the front of the cloaca (white lines). (B) Three layers of E15 hindgut: serosa, muscle layer, intestinal epithelium. Remak's ganglion was also removed. Scale bars: 1 mm in A, B

Supplementary Figure S2

(A) Co-staining of Day 7 organoids with anti-c-Kit- and Tuj1 antibodies. White arrowhead shows a $Tuj1^{+}$ cell. (B) Representation of $Tuj1^{+}$ cells in an organoid at day 7. Scale bar: 30 μm in A.

Supplementary Figure S3

(A) Day 7 organoid exhibited periodic contractions both before (0 μM; control) and after adding CBX. Graphs show contractions quantified by the difference in intensity of brightfield in sequential images. (B) Relative changes to the control in contraction frequency in day 7 organoid after CBX. The number is an average. Scale bar: 50 μm in A.

Movie 1

Long-term time-lapse imaging after seeding. Time lapse was taken every 2 hours for a total of 100 hours. This video corresponds to Fig. 1B.

Movie 2

Periodic contractions of the cluster/spheroid on day 3, 5 and 7. Time-lapse images were taken with 700 msec intervals for 5 min. This video corresponds to Fig. 2A.

Movie 3

Periodic contractions of a day 7 organoid with CBX. Time-lapse images were obtained with 700 msec intervals for 5 min. This video corresponds to Fig. S3.

Movie 4

Ca^{2+} dynamics in day 7 gut contractile organoid are concomitant with its contractions. Time-lapse images were obtained with 700 msec intervals for 5 min. This video corresponds to Fig. 4.

Movie 5

Ca^{2+} dynamics in a gut contractile organoid with CBX. Time-lapse images were obtained with 700 msec intervals for 5 min. This video corresponds to Fig. 5.

Movie 6

Ca^{2+} dynamics in day 7 gut contractile organoid with Blebbistatin. Time-lapse images were obtained with 700 msec intervals for 5 min. This video corresponds to Fig. 6.

Movie 7

Live imaging during fusion of multiple organoids. Time-lapse images were obtained every 10 minutes for 4 hours. This video corresponds to Fig. 7A.

Movie 8

Ca^{2+} transients in two gut contractile organoids before and after fusion. Time-lapse images were obtained with 450 msec intervals for 5 min. This video corresponds to Fig. 7B.

Movie 9

Ca^{2+} transients in three gut contractile organoids in 3-well hydrogel with channels. Time-lapse images were obtained with 700 msec intervals for 5 min. This video corresponds to Fig. 8C.

Movie 10

Ca^{2+} transients in three gut contractile organoids in 3-well hydrogel *without* channels. Time-lapse images were obtained with 450 msec intervals for 5 min. This video corresponds to Fig. 8G.

Movie 11

Similar assay to movie 10 with 18β-GA administration. Time-lapse images were obtained with 700 msec intervals for 5 min. This video corresponds to Fig. 8H.

Fig. 1

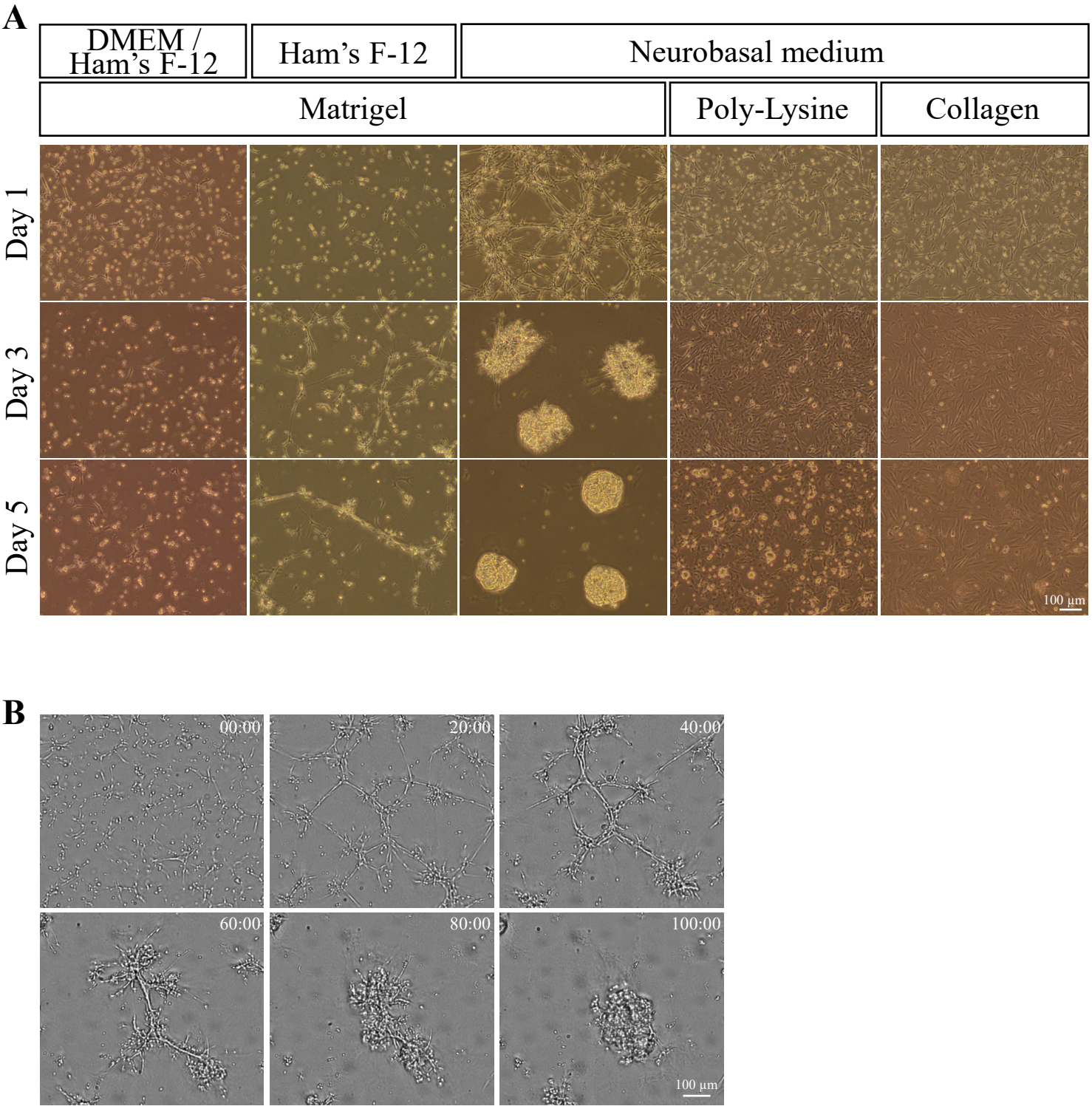
A
DMEM / Ham's F-12
Ham's F-12
Neurobasal medium
Matrigel
Poly-Lysine
Collagen
Day 1
Day 3
Day 5
100 µm
B
00:00
20:00
40:00
60:00
80:00
100:00
100 µm

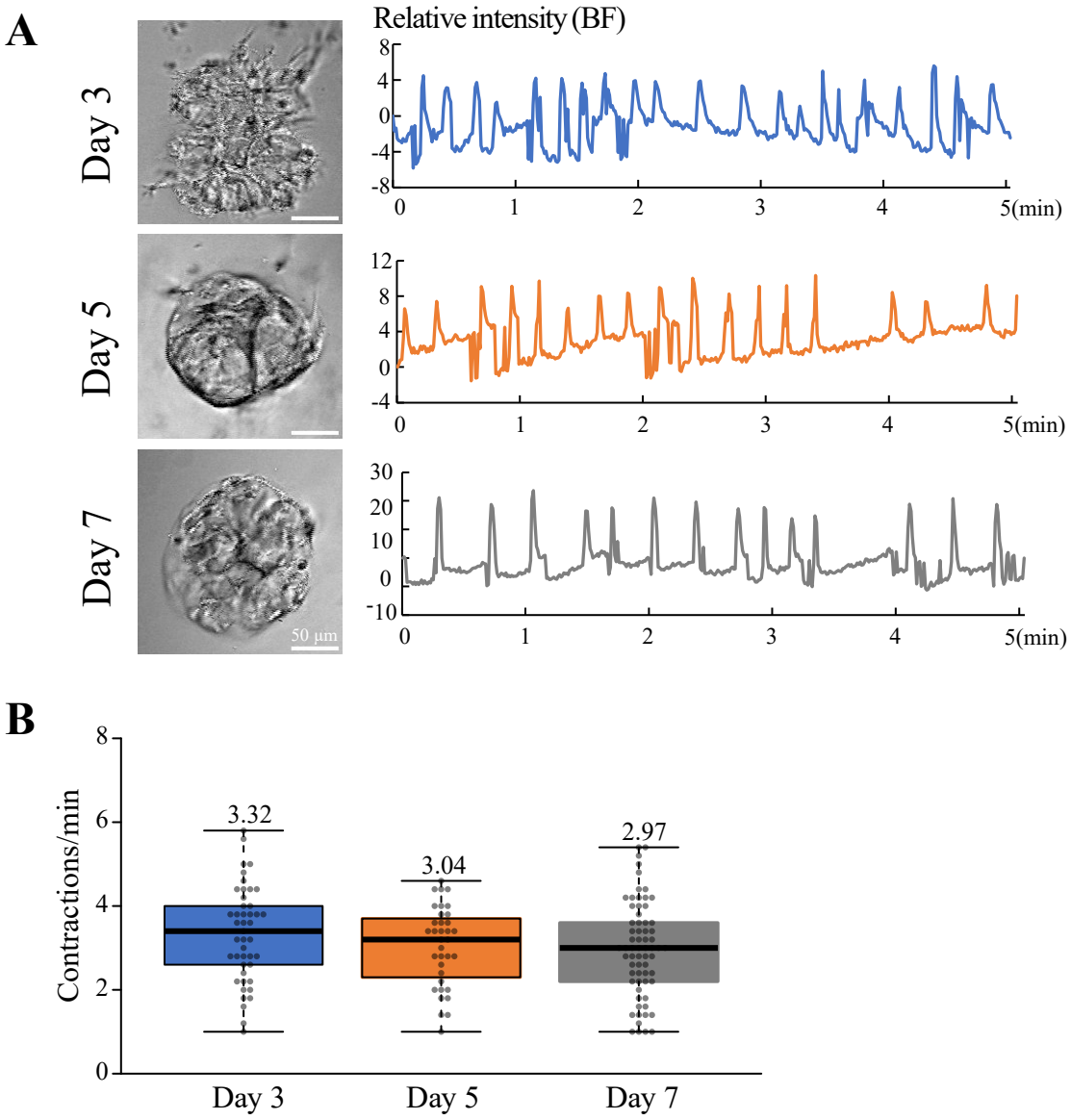
A
Relative intensity (BF)
Day 3
Day 5
Day 7
50 μm
8
4
0
-4
-8
12
8
4
0
-4
30
20
10
0
-10
0
1
2
3
4
5(min)
B
Contractions/min
8
6
4
2
0
3.32
3.04
2.97
Day 3
Day 5
Day 7

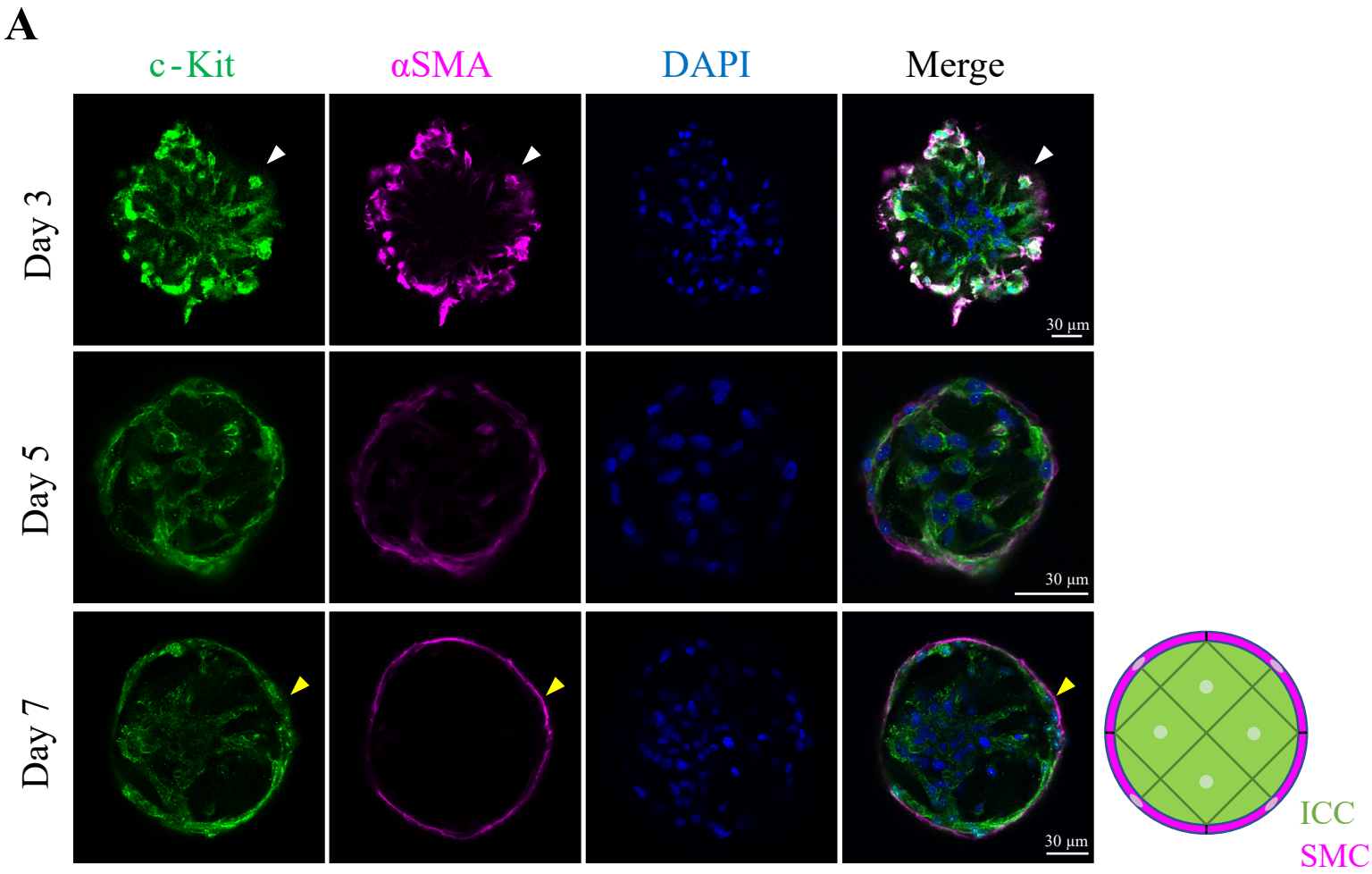
A
c-Kit
αSMA
DAPI
Merge
Day 3
Day 5
Day 7
30 μm
ICC
SMC

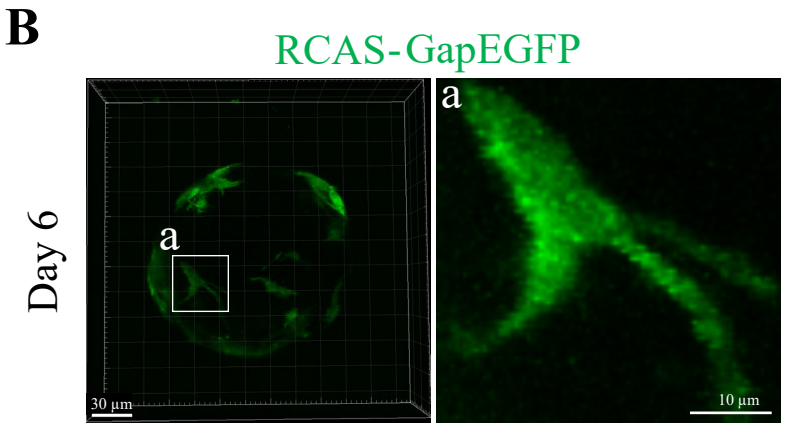
B
RCAS-GapEGFP
Day 6
a
30 μm
10 μm

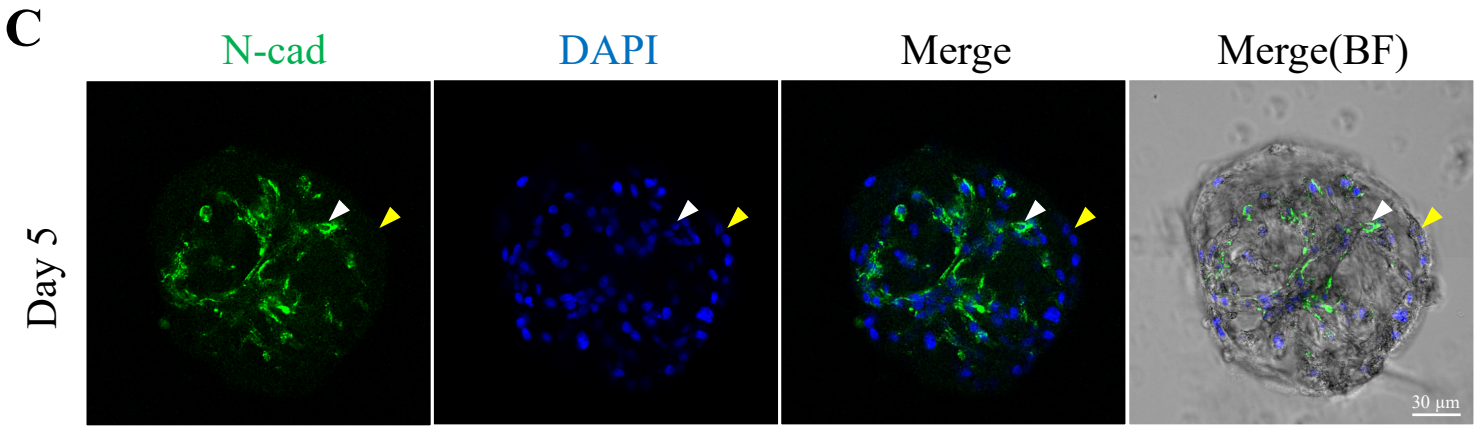
C
N-cad
DAPI
Merge
Merge(BF)
Day 5
30 μm

Fig. 4

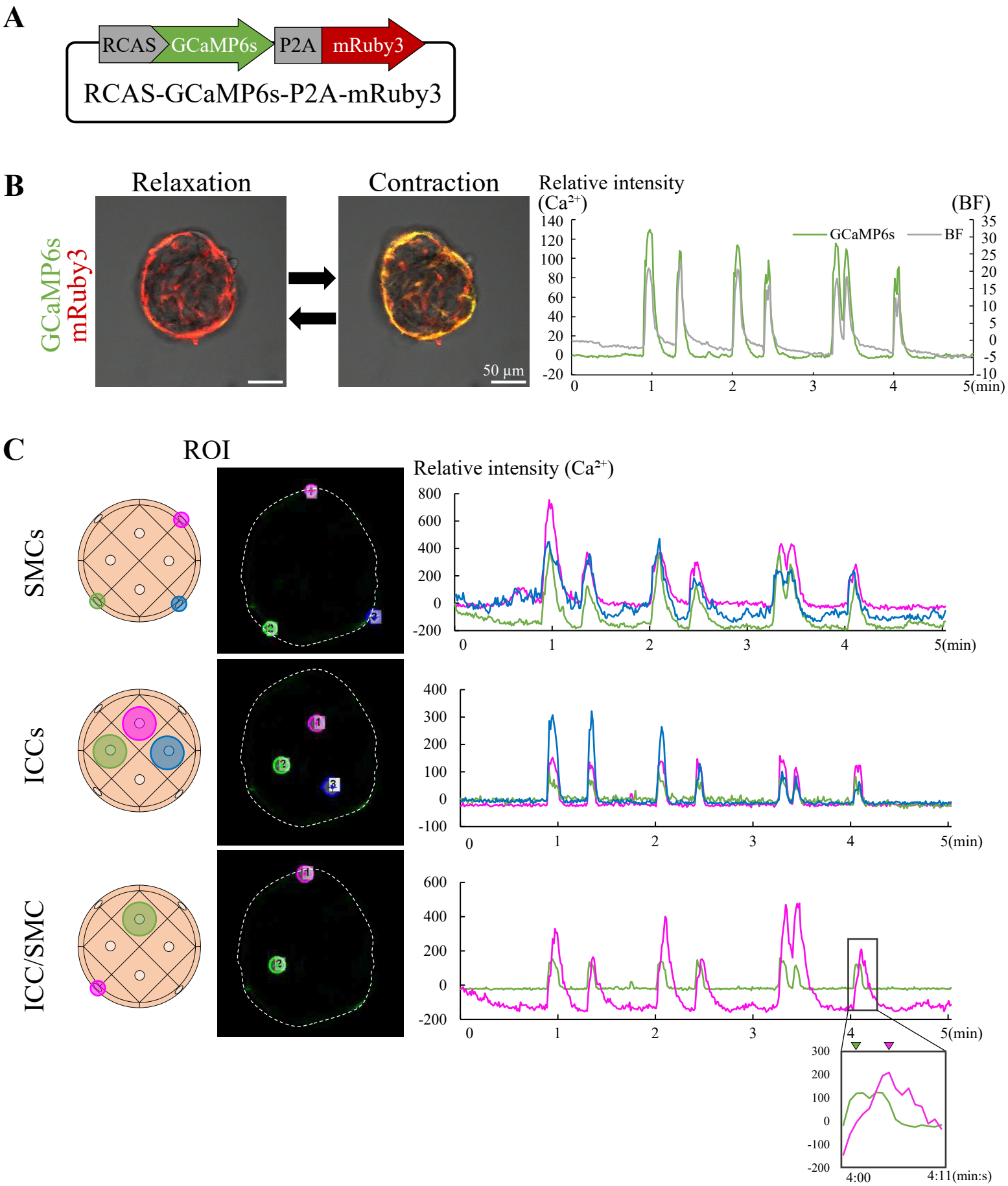
A
RCAS
GCaMP6s
P2A
mRuby3
RCAS-GCaMP6s-P2A-mRuby3
B
Relaxation
Contraction
GCaMP6s
mRuby3
50 μm
Relative intensity
(Ca²⁺)
(BF)
GCaMP6s
BF
5(min)
C
ROI
Relative intensity (Ca²⁺)
SMCs
ICCs
ICC/SMC
5(min)
4:00
4:11(min:s)

Fig.5

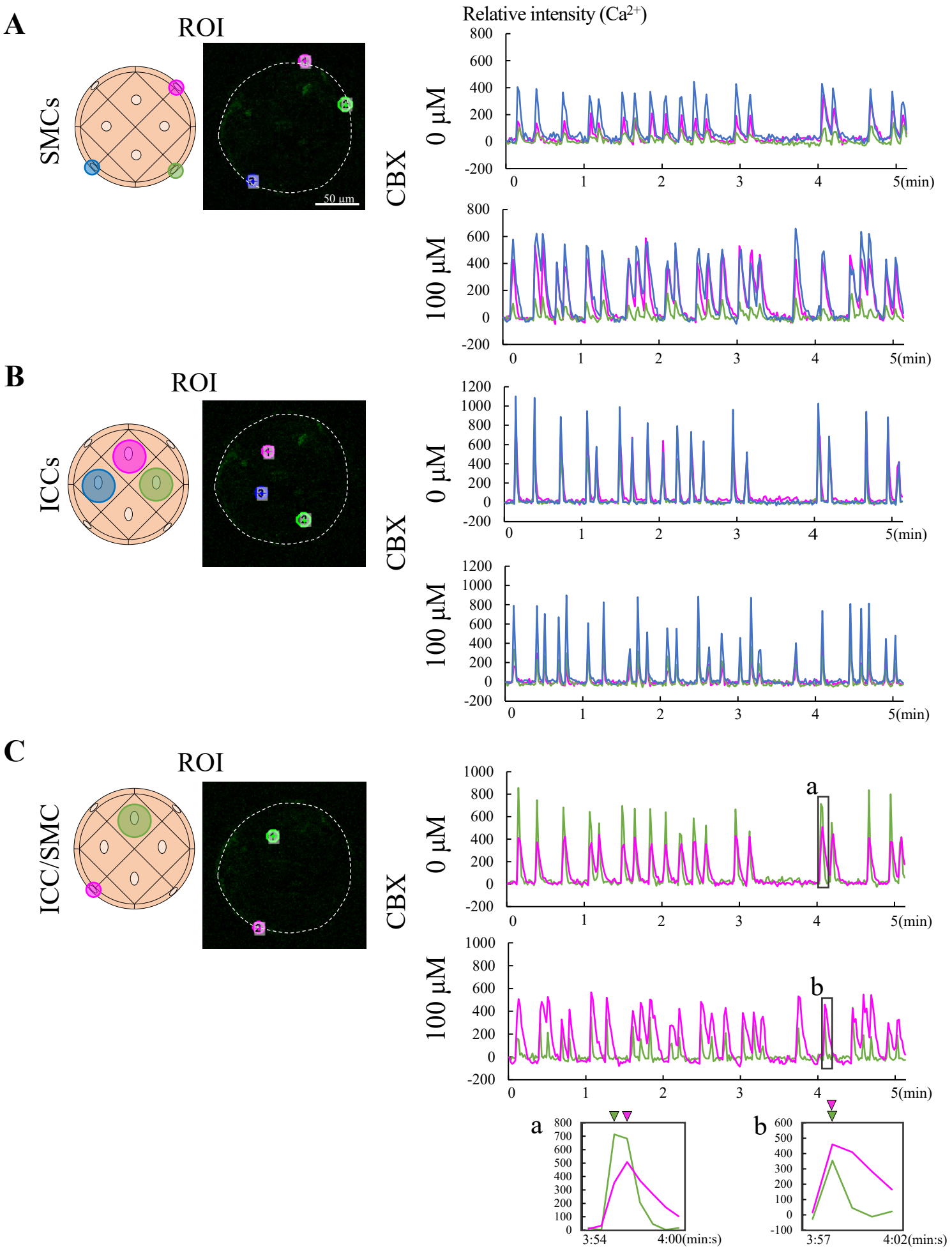
A
ROI
SMCs
50 μm
Relative intensity (Ca2+)
CBX
0 μM
100 μM
5(min)
B
ROI
ICCs
C
ROI
ICC/SMC
a
b
3:54
4:00(min:s)
3:57
4:02(min:s)

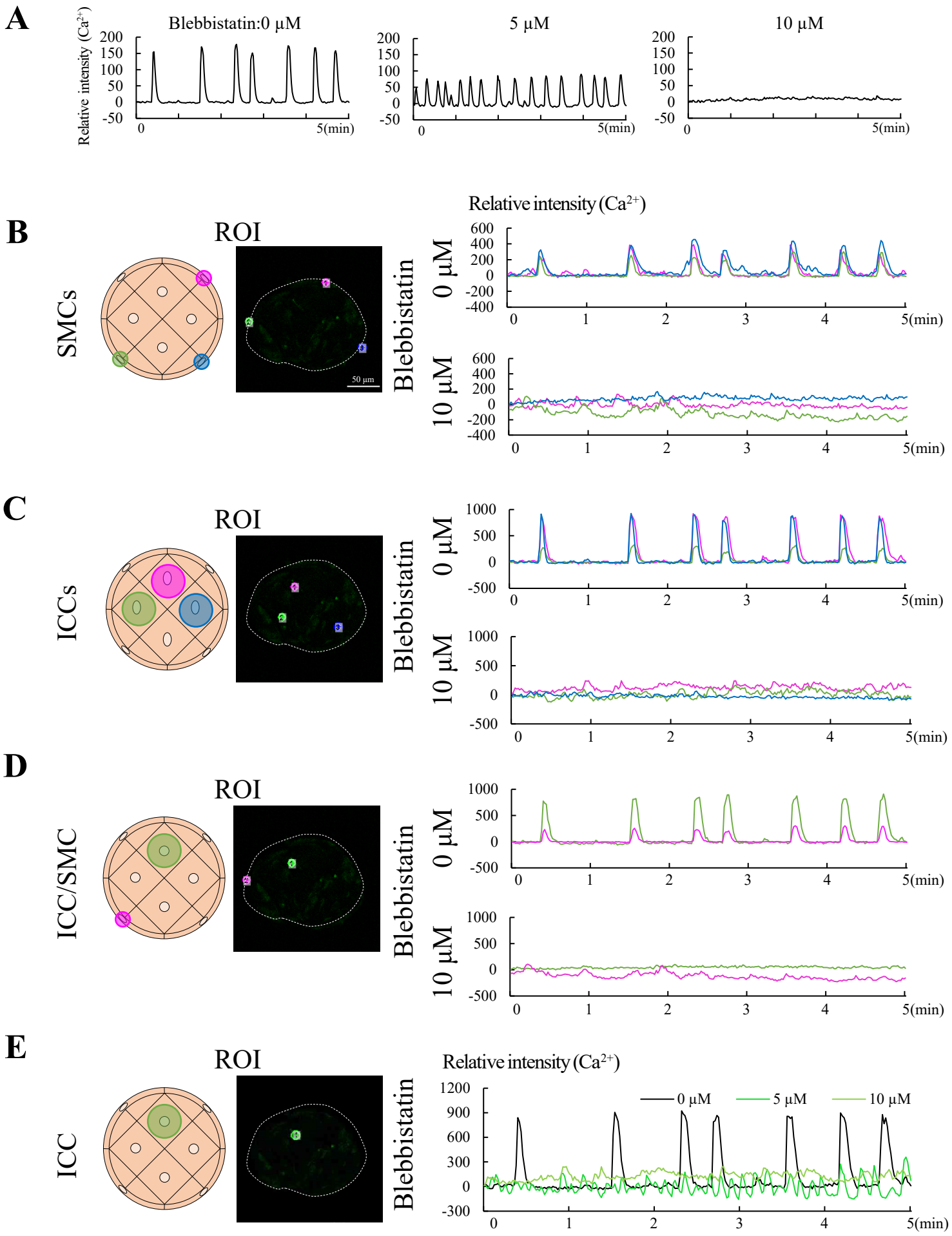
A
Blebbistatin:0 μM
5 μM
10 μM
Relative intensity (Ca2+)
200
150
100
50
0
-50
0
5(min)
B
SMCs
ROI
50 μm
Blebbistatin
0 μM
10 μM
Relative intensity (Ca2+)
600
400
200
0
-200
-400
0
1
2
3
4
5(min)
C
ICCs
ROI
Blebbistatin
0 μM
10 μM
1000
500
0
-500
D
ICC/SMC
ROI
Blebbistatin
0 μM
10 μM
E
ICC
ROI
Blebbistatin
Relative intensity (Ca2+)
0 μM
5 μM
10 μM
1200
900
600
300
0
-300

Fig. 7

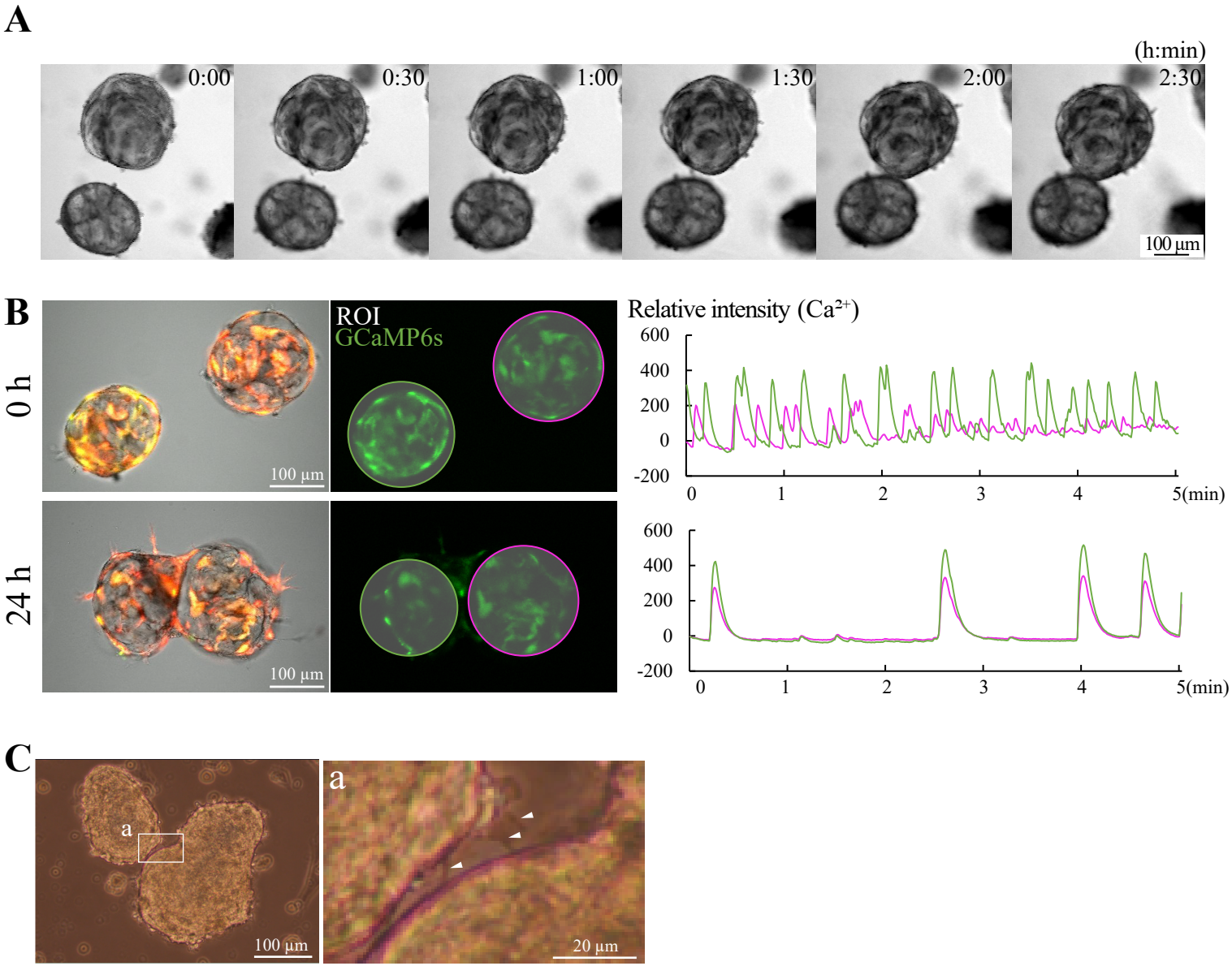
A
(h:min)
0:00
0:30
1:00
1:30
2:00
2:30
100 µm
B
0 h
24 h
ROI
GCaMP6s
100 µm
100 µm
Relative intensity (Ca²⁺)
600
400
200
0
-200
0
1
2
3
4
5(min)
C
a
100 µm
a
20 µm

Fig. 8

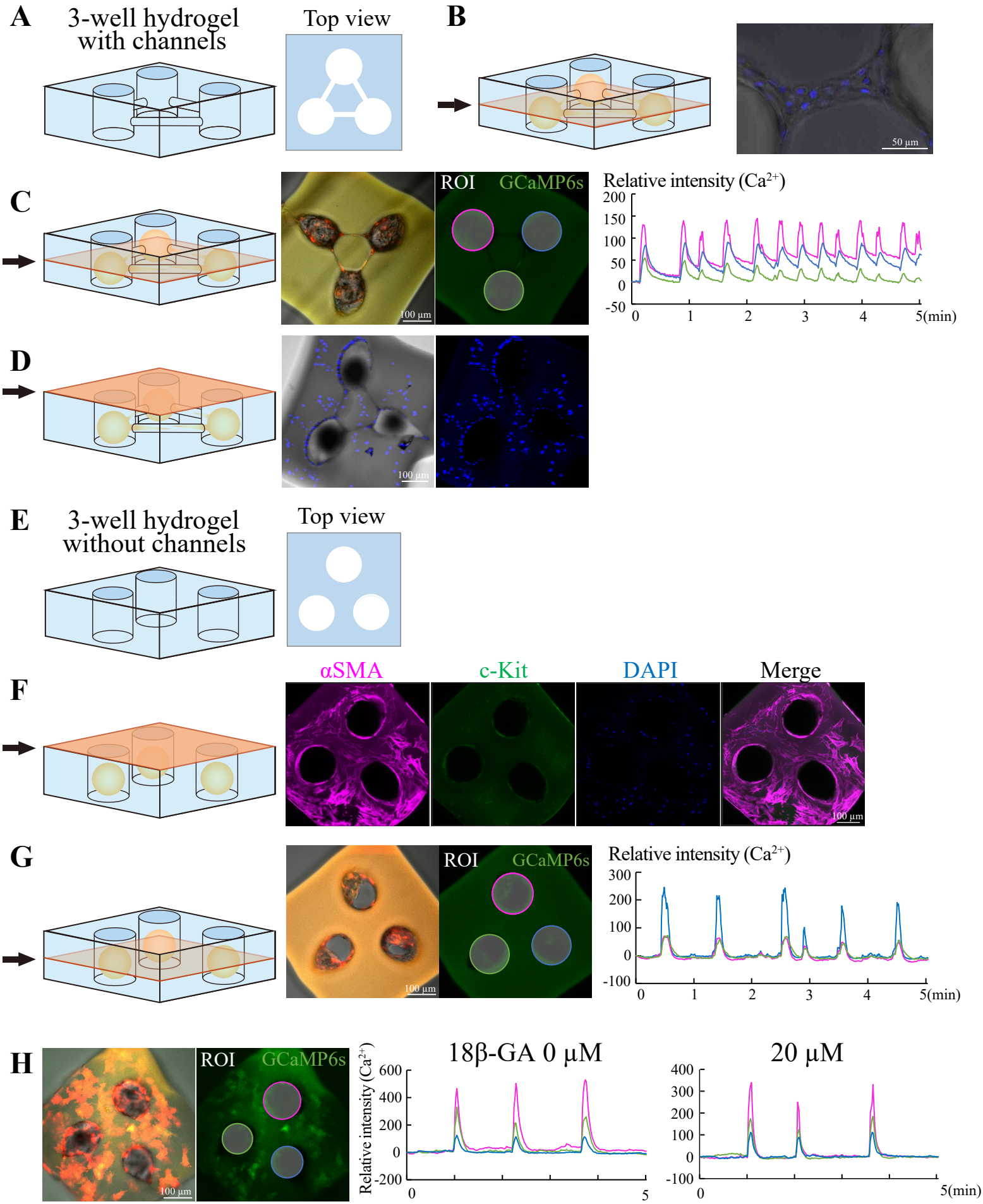
A
3-well hydrogel with channels
Top view
B
50 μm
C
ROI
GCaMP6s
100 μm
Relative intensity (Ca2+)
200
150
100
50
0
-50
0
1
2
3
4
5(min)
D
100 μm
E
3-well hydrogel without channels
Top view
F
αSMA
c-Kit
DAPI
Merge
100 μm
G
ROI
GCaMP6s
100 μm
Relative intensity (Ca2+)
300
200
100
0
-100
0
1
2
3
4
5(min)
H
ROI
GCaMP6s
100 μm
18β-GA 0 μM
20 μM
Relative intensity (Ca2+)
600
400
200
0
-200
0
5
400
300
200
100
0
-100
0
5(min)

Fig. S1

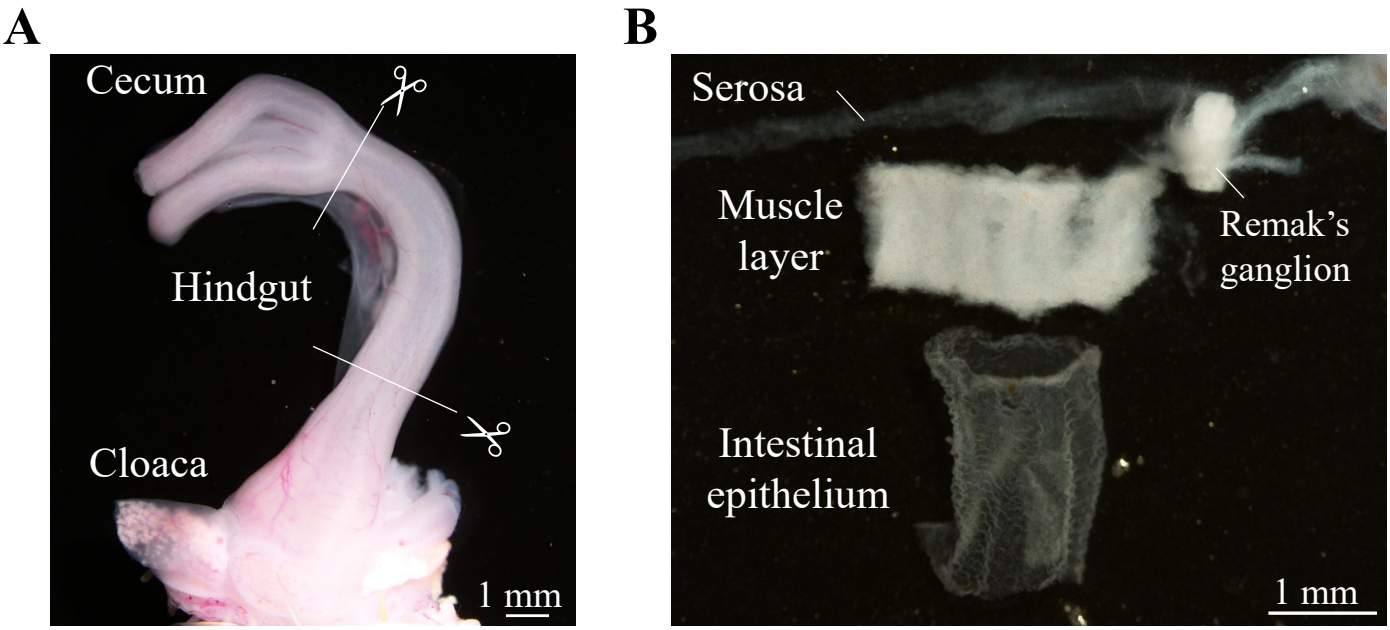
A
Cecum
Hindgut
Cloaca
1 mm
B
Serosa
Muscle layer
Remak's ganglion
Intestinal epithelium
1 mm

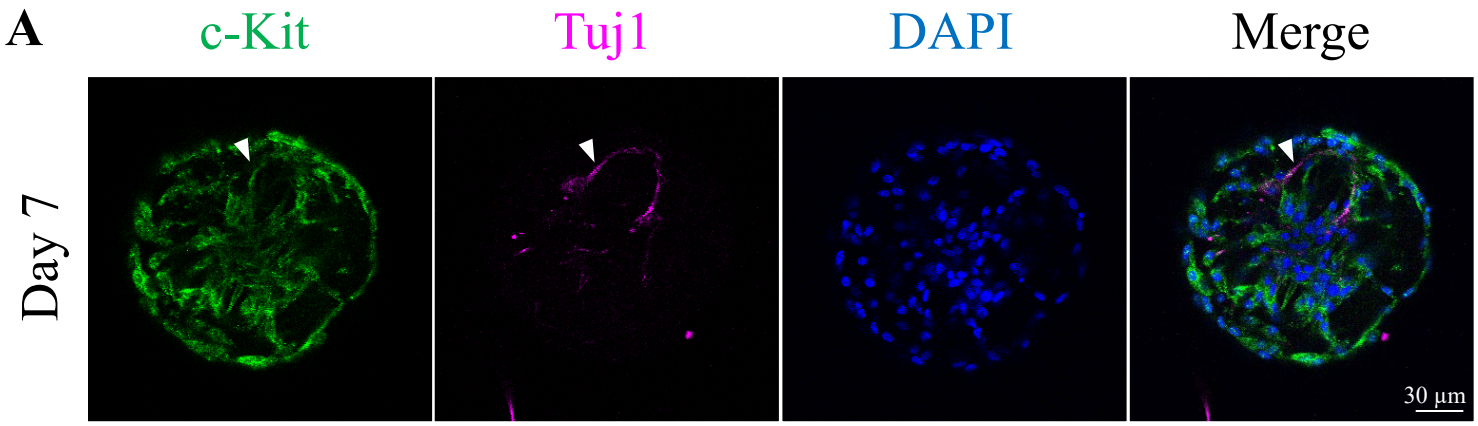
A
c-Kit
Tuj1
DAPI
Merge
Day 7
30 μm

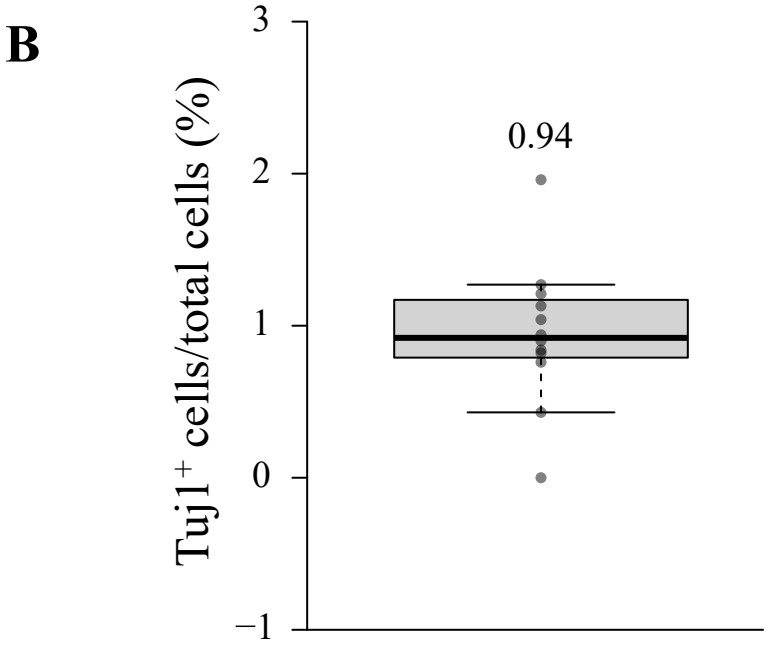
B
Tuj1+ cells/total cells (%)
3
2
1
0
−1
0.94

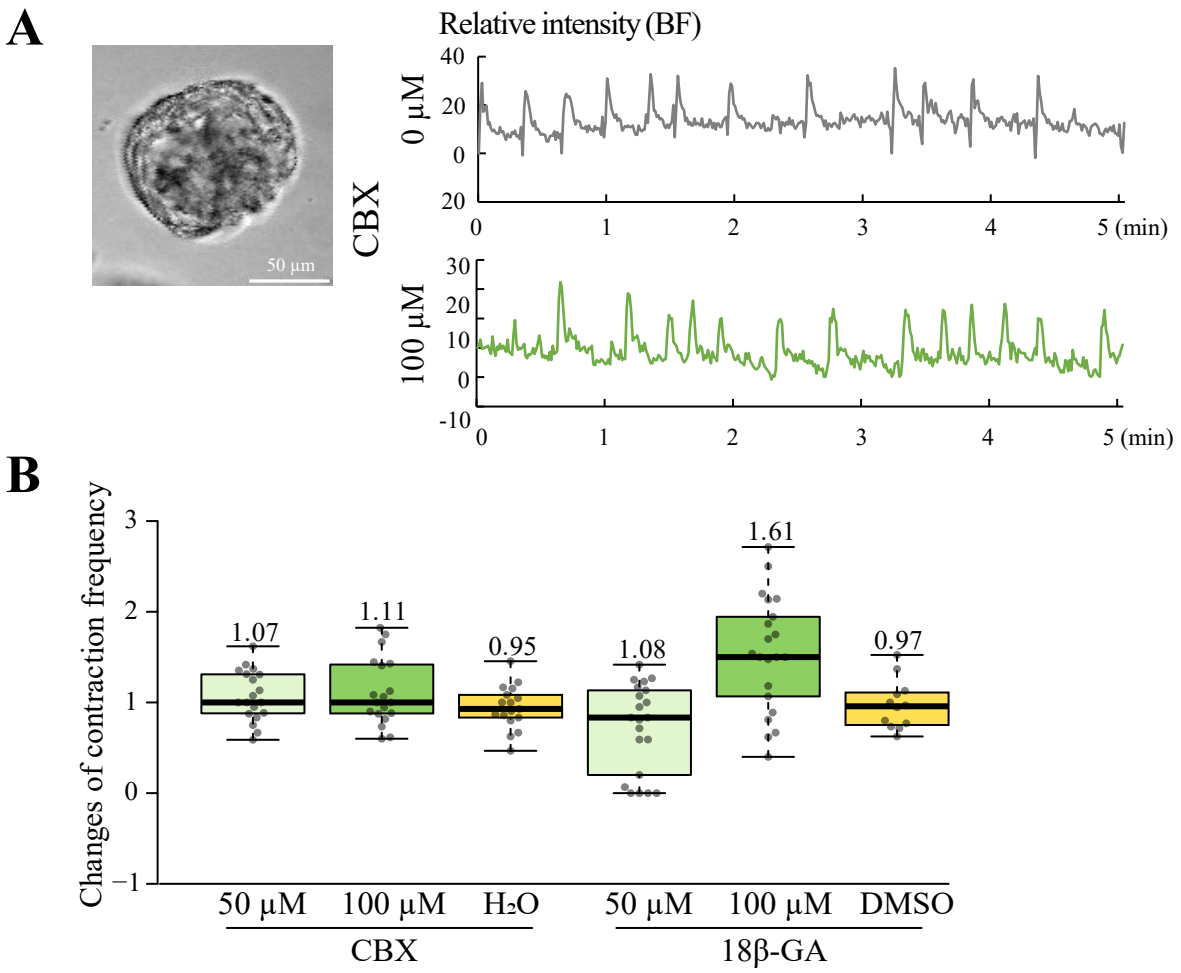
A
Relative intensity (BF)
50 μm
CBX
0 μM
100 μM
40
20
0
20
30
20
10
0
-10
0
1
2
3
4
5 (min)
B
Changes of contraction frequency
3
2
1
0
−1
1.07
1.11
0.95
1.08
1.61
0.97
50 μM
100 μM
H2O
50 μM
100 μM
DMSO
CBX
18β-GA